arXiv:1101.1382v1 [hep-ph] 7 Jan 2011

Mixing of Active and Sterile Neutrinos

Takehiko Asaka[1,2], Shintaro Eijima[3] and Hiroyuki Ishida[3]

[1] *Department of Physics, Niigata University, Niigata 950-2181, Japan*
[2] *Max-Planck-Institut für Kernphysik, Postfach 103980, 69029 Heidelberg, Germany*
[3] *Graduate School of Science and Technology, Niigata University, Niigata 950-2181, Japan*

January 10, 2011

Abstract

We investigate mixing of neutrinos in the νMSM (neutrino Minimal Standard Model), which is the MSM extended by three right-handed neutrinos. Especially, we study elements of the mixing matrix $\Theta_{\alpha I}$ between three left-handed neutrinos ν_α ($\alpha = e, \mu, \tau$) and two sterile neutrinos N_I ($I = 2, 3$) which are responsible to the seesaw mechanism generating the suppressed masses of active neutrinos as well as the generation of the baryon asymmetry of the universe (BAU). It is shown that Θ_{eI} can be suppressed by many orders of magnitude compared with $\Theta_{\mu I}$ and $\Theta_{\tau I}$, when the Chooz angle θ_{13} is large in the normal hierarchy of active neutrino masses. We then discuss the neutrinoless double beta decay in this framework by taking into account the contributions not only from active neutrinos but also from all the three sterile neutrinos. It is shown that N_2 and N_3 give substantial, destructive contributions when their masses are smaller than a few 100 MeV, and as a results Θ_{eI} receive no stringent constraint from the current bounds on such decay. Finally, we discuss the impacts of the obtained results on the direct searches of $N_{2,3}$ in meson decays for the case when $N_{2,3}$ are lighter than pion mass. We show that there exists the allowed region for $N_{2,3}$ with such small masses in the normal hierarchy case even if the current bound on the lifetimes of $N_{2,3}$ from the big bang nucleosynthesis is imposed. It is also pointed out that the direct search by using $\pi^+ \to e^+ + N_{2,3}$ and $K^+ \to e^+ + N_{2,3}$ might miss such $N_{2,3}$ since the branching ratios can be extremely small due to the cancellation in Θ_{eI}, but the search by $K^+ \to \mu^+ + N_{2,3}$ can cover the whole allowed region by improving the measurement of the branching ratio by a factor of 5.

1 Introduction

The extension by right-handed neutrinos is one of the most interesting physics beyond the Minimal Standard Model (MSM), since it gives a simple solution to the problem of the neutrino masses confirmed by various oscillation experiments. Usually, right-handed neutrinos are introduced with superheavy Majorana masses and sizable Yukawa coupling constants in order to realize the seesaw mechanism [1], which accounts naturally for the smallness of neutrino masses. Furthermore, the decays of such right-handed neutrinos can be a source of the baryon asymmetry of the universe (BAU) through the leptogenesis mechanism [2, 3]. When the masses of right-handed neutrinos are hierarchical, the observed BAU requires the mass of the lightest one should be heavier than about 10^9 GeV [4]. Although such singlet fermions provide simple and natural solution to the origins of neutrino masses and BAU at the same time, it is almost impossible to test them at experiments in the future.

It should, however, be noted that right-handed neutrinos can bring about important physical phenomena, even when the scale of Majorana masses are so light to be produced in terrestrial experiments. One attractive possibility is the νMSM [5, 6] in which three right-handed neutrinos are introduced with masses below the electroweak scale.[#1] Interestingly, this simple model can explain the origins of neutrino masses, BAU and also dark matter of the universe at the same time. The Yukawa coupling constants are so small that the seesaw mechanism still works, and mass eigenstates of neutrinos are divided into two groups, active and sterile neutrinos. The flavour mixing of active neutrinos accounts for neutrino oscillations observed in experiments. On the other hand, three sterile neutrinos, N_1, N_2, and N_3, solve cosmological problems in the MSM.

One of the sterile neutrinos, N_1, plays a role of dark matter [14].[#2] When its mass is in the keV order, it can be produced by the so-called Dodelson-Widrow mechanism [17], *i.e.*, by the thermal scatterings through its mixing with the left-handed neutrinos. See Refs. [18]–[27]. This dark-matter particle receives severe astrophysical constraints [28]. One important bound comes from the X-ray background [19]–[21] and the other comes from the cosmic structure at small scales like the Lyman α forest [29]–[32]. Even when these constraints are imposed, as shown in Ref. [27], the correct abundance of the dark matter can be obtained through the Dodelson-Widrow mechanism by invoking the resonant production [18] in the presence of the large lepton asymmetry. Notice that N_1 plays no significant role in the seesaw mechanism [5]. This is because Yukawa coupling constants of N_1 is so small that its contribution to the mass matrix of active neutrinos is negligible. Due to the very suppressed interaction the direct search of N_1 at experiments is very difficult. However, it can be observed by the specific spectrum in

[#1] The explanation of the LSND anomaly in this framework had been investigated in Ref. [7]. The non-minimal coupling of the Higgs field to gravity allows to realize the cosmic inflation [8]. Further, various extensions of the model have been discussed [9]-[13].

[#2] It has been investigated various phenomenon in astrophysics by the sterile neutrino dark-matter, *e.g.*, the explanation of the pulsar kick [15]. See, for example, a review of this issue [16] and references therein.

the X-ray background coming from the decay of N_1 into active neutrino and photon. It has also been discussed the search in laboratory [33].

The rest two sterile neutrinos, N_2 and N_3, are responsible to generate not only the seesaw masses of active neutrinos but also BAU through the mechanism [34]. The flavour oscillation between N_2 and N_3 in the early universe induces the separation of lepton asymmetry between left- and right-handed leptons and the asymmetry in the left-handed sector is partially converted into the baryon asymmetry by the sphaleron processes [35]. The νMSM realizes this baryogenesis scenario without conflict with the observational data of the neutrino oscillations when their masses are quasi-degenerate and in the range $\mathcal{O}(0.1)$–$\mathcal{O}(10)$ GeV [6]. See also the recent analysis in Refs. [36, 37].

It is interesting to note that sterile neutrinos N_2 and N_3 can be tested in various experiments as pointed out in Ref. [38]. This is crucially important to reveal the origins of the neutrino masses as well as the cosmic baryon asymmetry. For this purpose, we would like to study the mixing of sterile neutrinos with left-handed neutrinos ν_α ($\alpha = e, \mu, \tau$) in this paper. The elements of such mixing matrix, $\Theta_{\alpha I}$, are vital to discuss phenomenology of the νMSM, since the strength of the interactions of sterile neutrinos is determined by them. Sterile neutrinos in the model possess the Yukawa interactions and also the weak gauge interactions via the above mixing after the electroweak symmetry breaking. Since the elements $\Theta_{\alpha I}$ are proportional to the Yukawa coupling constants $F_{\alpha I}$, both interactions are controlled by $\Theta_{\alpha I}$.

It should be noted that the mixing elements of N_2 and N_3 can take values varying by many orders of magnitude. This point had already been discussed by using the model with the lepton symmetry [39]. As we will show in Sec. 3, the mixing elements increase exponentially as $\Theta_{\alpha I} \propto \exp(\mathrm{Im}\omega)$ for large $\mathrm{Im}\omega$ (ω is a complex parameter in the neutrino Yukawa matrix) keeping the masses and mixing angles of active neutrinos unchanged. This enhancement leads to the various significant impacts on phenomenology of sterile neutrinos. For example, it gives the larger production/detection rates in the search experiments, the larger CP asymmetry in baryogenesis, and the shorter lifetime of $N_{2,3}$ making them cosmologically harmless.

The purpose of this paper is, thus, to investigate the mixing elements $\Theta_{\alpha I}$ in detail, and to reveal how the elements of N_2 and N_3 depend on mass hierarchy, mixing angles and CP phases of active neutrinos in addition to the parameters of sterile neutrinos. Our analysis will show that there can be strong hierarchy among the mixing elements Θ_{eI}, $\Theta_{\mu I}$ and $\Theta_{\tau I}$ depending on choice of the parameters. Especially, it will been pointed out that the strong suppression in the mixing elements of electron type Θ_{eI} can happen for the normal hierarchy of active neutrino masses, which enlarges the allowed region of the model. Although we shall consider the νMSM, the results of the mixing elements $\Theta_{\alpha I}$ in this paper can be applied to the general models of the seesaw mechanism with two right-handed neutrinos.

Further, we would like to discuss the implications to two phenomena of sterile neutrinos. The first one is the neutrinoless double beta decay in which the mixing elements of active and sterile neutrinos play the crucial roles. This problem had already been discussed in Ref. [40].

We will extend the analysis especially when the masses of N_2 and N_3 are smaller than a few 100 MeV, and show that the rates of the decays in the νMSM is smaller than those in the usual case where only active neutrinos give the contribution. Thus, the model is free from significant constraints discussed in Ref. [41]. The other one is the search of $N_{2,3}$ produced in the decays of charged pions and/or kaons where the elements $|\Theta_{eI}|^2$ or $|\Theta_{\mu I}|^2$ determine the production rates. Especially, we will point out that N_2 and N_3 which masses are smaller than pion mass are still allowed by the constraints from the direct searches as well as that from the big bang nucleosynthesis [42, 43] for the normal hierarchy case. This is different from a conclusion from Ref. [38]. The reason for it lies in the cancellation in the Θ_{eI} mentioned above. In addition, we shall present some implications to the future searches by using the decays of π^+ and K^+.

This paper is organized as follows. In Sec. 2 we briefly review the framework of the present analysis, *i.e.*, the νMSM. In Sec. 3 we study the mixing of sterile neutrinos N_2 and N_3 in the charged current interactions. Especially, we investigate how the mixing elements depend on the parameters of active neutrinos, *i.e.*, the mass hierarchy, mixing angles and CP violating phases. We then apply the obtained results in phenomenology of N_2 and N_3. In Sec. 4 we estimate the contributions of sterile neutrinos to the neutrinoless double beta decay and address the importance of such contributions when the masses of N_2 and N_3 are smaller than about the order of 100 MeV. In Sec. 5 we discuss search of N_2 and N_3 in the charged pion and kaon decays for the case when their masses are lighter than the pion mass. Finally, our results are summarized in Sec. 6. We add App. A to present the expressions for the mixing elements.

2 The νMSM

First of all, we review the νMSM, which is the MSM extended by three right-handed neutrinos $\nu_{R\,I}$ $(I = 1, 2, 3)$ with Lagrangian

$$\mathcal{L}_{\nu\text{MSM}} = \mathcal{L}_{\text{MSM}} + i\,\overline{\nu_{RI}}\,\gamma^\mu\,\partial_\mu\,\nu_{RI} - \left(F_{\alpha I}\,\overline{L}_\alpha\,\Phi\,\nu_{RI} + \frac{M_I}{2}\,\overline{\nu_{RI}^c}\,\nu_{RI} + h.c.\right), \tag{1}$$

where $\mathcal{L}_{\text{MSM}}$ is the MSM Lagrangian. Φ and $L_\alpha = (e_{L\,\alpha}, \nu_{L\,\alpha})^T$ $(\alpha = e, \mu, \tau)$ are Higgs and lepton weak-doublets, respectively. We denote Yukawa coupling constants of neutrinos by $F_{\alpha I}$. Here and hereafter we work in a basis in which the mass matrix of charged leptons is diagonal. In this model neutrinos receive the Majorana masses $[M_M]_{IJ} = M_I\delta_{IJ}$ (which are taken to be real and positive without loss of generality) and the Dirac masses $[M_D]_{\alpha I} = F_{\alpha I}\langle\Phi\rangle$ ($\langle\Phi\rangle$ is a vacuum expectation value of the Higgs field). The distinctive feature of the model is the region of the parameter space of Eq. (1), *i.e.*, we restrict ourselves in the region

$$|[M_D]_{\alpha I}| \ll M_I \lesssim \Lambda_{\text{EW}}\ . \tag{2}$$

Notice that the seesaw mechanism still works even if the Majorana masses are smaller than or comparable to the weak scale $\Lambda_{\text{EW}} = \mathcal{O}(10^2)$ GeV. This is simply because neutrino Yukawa coupling constants of interest are extremely small. (See the discussion below.)

The mass matrix of neutrinos $\hat{M}$, which is a 6×6 symmetric matrix, is given by

$$\hat{M} = \begin{pmatrix} 0 & M_D \\ M_D^T & M_M \end{pmatrix} . \tag{3}$$

We can diagonalize it by using the unitary matrix $\hat{U}$ as $\hat{U}^\dagger \hat{M} \hat{U}^* = \hat{M}^{\rm diag}$. The seesaw mechanism shows that $\hat{U}$ at the leading order takes the form

$$\hat{U} = \begin{pmatrix} U & \Theta \\ -\Theta^\dagger U & 1 \end{pmatrix} . \tag{4}$$

Here U is the 3×3 Pontecorvo-Maki-Nakagawa-Sakata (PMNS) matrix [44];

$$U^\dagger M_\nu U^* = {\rm diag}(m_1, m_2, m_3) \, , \tag{5}$$

where $M_\nu = -M_D M_M^{-1} M_D^T$ is the seesaw mass matrix. We call the eigenstates having masses m_i as active neutrinos ν_i $(i = 1, 2, 3)$. The rest three mass eigenstates, denoted by N_I, are almost corresponding to right-handed neutrinos $N_I \simeq \nu_{R\,I}$ having masses M_I. The neutrino mixing in the charge current is then induced through

$$\nu_{L\alpha} = U_{\alpha i} \, \nu_i + \Theta_{\alpha I} \, N_I^c \, , \tag{6}$$

where the 3×3 mixing matrix Θ is found at the leading order as

$$\Theta_{\alpha I} = \frac{[M_D]_{\alpha I}}{M_I} \, , \tag{7}$$

and hence $|\Theta_{\alpha I}| \ll 1$ due to Eq. (2). We shall call N_I as sterile neutrinos since they possess very suppressed gauge interactions. It should be stressed that sterile neutrinos here are originated from right-handed neutrinos in the seesaw mechanism.

In the νMSM three right-handed neutrinos play important roles in cosmology. One of them, say N_1, is a candidate for dark matter of the universe. This dark-matter particle receives severe astrophysical constraints as mentioned in Sec. 1. Even then, the correct dark-matter abundance can be obtained through the mechanism [17] with the resonant production [18] in the presence of the large lepton asymmetry. The recent study [27] shows that the required mass is $M_1 = 4$–50 keV and the Yukawa coupling constants are typically $|F_{\alpha 1}| = 5 \times 10^{-15}$–$4 \times 10^{-13}$. As a result, N_1 gives no significant contribution to the seesaw mass matrix M_ν [5].

The other right-handed neutrinos, N_2 and N_3, are then responsible to the masses and mixing of active neutrinos. Notice that in this case the mass of the lightest active neutrino becomes $m_1 < \mathcal{O}(10^{-6})$ eV. Further, N_2 and N_3 can explain the origin of BAU. The flavour oscillation between them in the early universe can generate BAU through the mechanism proposed in Ref. [34]. In the νMSM the correct amount of BAU can be obtained when N_2 and N_3 are quasi-degenerate in mass [6, 36, 37].

The main purpose of this paper is to study the mixing elements $\Theta_{\alpha I}$ $(I = 2, 3)$ of sterile neutrinos N_2 and N_3 with flavour neutrinos. To do this, let us express their Yukawa coupling

constants by using mixing angles and masses of active neutrinos in oscillation experiments. As mentioned before, the successful dark matter scenario requires very small Yukawa couplings of N_1 and its contribution to M_ν can be neglected. Thus, we set $F_{\alpha 1} = 0$ here for simplicity. (See, however, the discussion in Sec. 4.) In this case the neutrino Yukawa matrix F for N_2 and N_3, which is a 3×2 matrix, can be expressed without loss of generality as [45, 46]

$$F = \frac{i}{\langle \Phi \rangle} U D_\nu^{1/2} \Omega D_N^{1/2} . \tag{8}$$

Here parameters of active neutrinos are their masses $D_\nu = \mathrm{diag}(m_1, m_2, m_3)$ and the mixing matrix

$$U = \begin{pmatrix} c_{12}c_{13} & s_{12}c_{13} & s_{13}e^{-i\delta} \\ -c_{23}s_{12} - s_{23}c_{12}s_{13}e^{i\delta} & c_{23}c_{12} - s_{23}s_{12}s_{13}e^{i\delta} & s_{23}c_{13} \\ s_{23}s_{12} - c_{23}c_{12}s_{13}e^{i\delta} & -s_{23}c_{12} - c_{23}s_{12}s_{13}e^{i\delta} & c_{23}c_{13} \end{pmatrix} \times \mathrm{diag}(1\,,\ e^{i\eta}\,,\ 1)\,, \tag{9}$$

with $s_{ij} = \sin\theta_{ij}$ and $c_{ij} = \cos\theta_{ij}$. Note that there is one Majorana phase η in addition to Dirac phase δ under the considering situation. Because we have set $F_{\alpha 1} = 0$, masses of active neutrinos are

$$\begin{aligned} &m_3 = m_{\rm atm} > m_2 = m_{\rm sol} > m_1 = 0 \quad \text{in the NH case}\,, \\ &m_2 = \sqrt{m_{\rm atm}^2 + m_{\rm sol}^2} > m_1 = \sqrt{m_{\rm atm}^2} > m_3 = 0 \quad \text{in the IH case}\,, \end{aligned} \tag{10}$$

The observational data of mixing angles are $s_{12}^2 = 0.318^{+0.062}_{-0.048}$, $s_{23}^2 = 0.50^{+0.17}_{-0.14}$, and $s_{13}^2 \leq 0.053$, respectively, and masses are $m_{\rm sol}^2 = \Delta m_{21}^2 = (7.59^{+0.68}_{-0.56}) \times 10^{-5}$ eV^2 and $m_{\rm atm}^2 = |\Delta m_{31}^2| = (2.40^{+0.35}_{-0.33}) \times 10^{-3}$ eV^2 (at the 3σ level) [47]. Hereafter, we shall adopt the central values unless otherwise stated.

On the other hand, parameters of N_2 and N_3 are their masses $D_N = \mathrm{diag}(M_2, M_3)$ and the 3×2 matrix

$$\begin{aligned} \Omega &= \begin{pmatrix} 0 & 0 \\ \cos\omega & -\sin\omega \\ \xi\sin\omega & \xi\cos\omega \end{pmatrix} \quad \text{in the NH case}\,, \\ \Omega &= \begin{pmatrix} \cos\omega & -\sin\omega \\ \xi\sin\omega & \xi\cos\omega \\ 0 & 0 \end{pmatrix} \quad \text{in the IH case}\,, \end{aligned} \tag{11}$$

where $\xi = \pm 1$ and ω is an arbitrary complex number. Notice that the change of the sign ξ can be compensated by $\omega \to -\omega$ together with the redefinition of N_3 as $\xi N_3 \to N_3$ [46].

3 Mixing matrix of sterile neutrinos

The important parameters for phenomenology of sterile neutrinos N_2 and N_3 are their masses $M_{2,3}$ and mixing matrix Θ. Especially, the latter one is crucial to specify the strength of

interactions with other particles. Here we would like to discuss how they depends on the parameters of active neutrinos.

Before discussing the νMSM, let us consider a toy model with one pair of left- and right-handed neutrinos. In this case, the mixing of sterile neutrino is given by [cf. Eq. (4)]

$$|\Theta|^2 = \frac{|M_D|^2}{M_N^2} = \frac{M_\nu}{M_N} = 4.9 \times 10^{-11} \left(\frac{1\ \text{GeV}}{M_N}\right) \left(\frac{M_\nu^2}{2.4 \times 10^{-3}\ \text{eV}^2}\right)^{1/2} , \tag{12}$$

where M_D and M_N are the Dirac and Majorana masses, and we have used the seesaw formula for active neutrino mass $M_\nu = |-M_D^2/M_N|$. Thus, the mixing is determined from the masses of active and sterile neutrinos.

In the νMSM, since the parameter space is larger, the mixing matrix of N_2 and N_3 is more complicated and its elements can be much different from Eq. (12). Especially, as pointed out in Ref. [39], the larger mixing can be obtained in the model with U(1) symmetry. We shall reanalyze this point by using the parametrization of the Yukawa matrix F presented in Eq. (8). The key for this issue is the complex parameter ω in the Ω matrix. It can be seen that the Yukawa coupling constants as well as the elements of mixing matrix become exponentially large as $F_{\alpha I}, \Theta_{\alpha I} \propto \exp(|\text{Im}\omega|)$ for $|\text{Im}\omega| \gg 1$, as long as the seesaw approximation is valid. It should be noted that the tiny neutrino masses observed in the oscillation experiments can be obtained even in this case. To express this enhancement factor, we introduce a parameter X_ω by

$$X_\omega = \exp(\text{Im}\omega) . \tag{13}$$

Before going into details, let us here summarize the general properties of mixing elements $\Theta_{\alpha I}$.

(i) $|\Theta_{\alpha I}|^2$ can be divided into X_ω^2, X_ω^0 and X_ω^{-2} terms.

(ii) The X_ω^2 term in $|\Theta_{\alpha 2}|^2 M_2$ is exactly the same as that in $|\Theta_{\alpha 3}|^2 M_3$ for $\alpha = e, \mu, \tau$. Similarly, the X_ω^{-2} term in $|\Theta_{\alpha 2}|^2 M_2$ is exactly the same as that in $|\Theta_{\alpha 3}|^2 M_3$.

(iii) The X_ω^0 term in $|\Theta_{\alpha 2}|^2 M_2$ is opposite to that in $|\Theta_{\alpha 3}|^2 M_3$ for $\alpha = e, \mu, \tau$.

(iv) The coefficient of the X_ω^{-2} term in $|\Theta_{\alpha I}|^2 M_I$ is obtained from the X_ω^2 term by changing $\xi \to -\xi$ for $\alpha = e, \mu, \tau$ and $I = 2, 3$.

We have confirmed these properties by direct calculations. From now on, we will present the expressions of $|\Theta_{\alpha I}|^2$ for $|\text{Im}\omega| \gg 1$ and discuss how they depend on the neutrino parameters, namely mass hierarchy, mixing angles, and CP violating phases of active neutrinos.

We first consider $|\Theta_{\alpha I}|^2$ for $X_\omega \gg 1$ (*i.e.*, $\text{Im}\omega \gg 1$) in the NH case. The leading $\mathcal{O}(X_\omega^2)$ terms are found as

$$|\Theta_{eI}|^2\big|_{X_\omega^2} = X_\omega^2 \frac{m_{\text{atm}}}{4M_I} \cos^2\theta_{13} \left[\tan^2\theta_{13} + 2\sqrt{r_m}\xi \sin(\delta+\eta) \sin\theta_{12}\ \tan\theta_{13} + r_m \sin^2\theta_{12}\right] , \tag{14}$$

$$|\Theta_{\mu I}|^2\big|_{X_\omega^2} = X_\omega^2 \frac{m_{\text{atm}}}{4M_I}\ \sin^2\theta_{23}\ \cos^2\theta_{13} \left[1 + \mathcal{O}(\sqrt{r_m})\right] , \tag{15}$$

$$|\Theta_{\tau I}|^2\big|_{X_\omega^2} = X_\omega^2 \frac{m_{\text{atm}}}{4M_I}\ \cos^2\theta_{23}\ \cos^2\theta_{13} \left[1 + \mathcal{O}(\sqrt{r_m})\right] , \tag{16}$$

where $r_m = m_{\rm sol}/m_{\rm atm} \simeq 0.18$. (The complete expressions for the $\mathcal{O}(X_\omega^2)$ terms are collected in App. A.) Notice that these expressions hold for both $I = 2$ and 3 thanks to the general property (ii). It is seen that all the elements are proportional to $X_\omega^2 m_{\rm atm}/M_I$, and hence they can be much larger than Eq. (12) for $X_\omega \gg 1$.

Since the experiments show that θ_{13} is small and θ_{23} is close to $\pi/4$, $|\Theta_{\mu I}|^2$ and $|\Theta_{\tau I}|^2$ can be determined as

$$|\Theta_{\mu I}|^2 \simeq |\Theta_{\tau I}|^2 \simeq X_\omega^2 \frac{m_{\rm atm}}{8M_I} = 6.1 \times 10^{-12}\, X_\omega^2 \left(\frac{1\ {\rm GeV}}{M_I}\right) . \tag{17}$$

On the other hand, the element Θ_{eI} behaves quite differently. Indeed, it is interesting to note that the X_ω^2 terms in $|\Theta_{e2}|^2$ and $|\Theta_{e3}|^2$ vanish at the same time, when

$$\xi \sin(\delta + \eta) = -1 , \tag{18}$$

and the mixing angle θ_{13} takes its critical value $\theta_{13}^{\rm cr}$:

$$\tan\theta_{13}^{\rm cr} = \sqrt{r_m} \sin\theta_{12} . \tag{19}$$

The experimental data of θ_{12}, $m_{\rm atm}$ and $m_{\rm sol}$ with 3σ errors gives the critical value of θ_{13} as $\sin^2\theta_{13}^{\rm cr} = 0.041$–$0.070$, which can be below the 3σ upper bound $\sin^2\theta_{13} < 0.053$.[#3] Moreover, we find in this case that the $\mathcal{O}(X_\omega^0)$ term also vanishes and only the $\mathcal{O}(X_\omega^{-2})$ term is left as

$$|\Theta_{eI}|^2 \simeq X_\omega^{-2} \frac{m_{\rm atm} r_m}{M_I} \sin^2\theta_{12} \simeq 2.8 \times 10^{-12}\, X_\omega^{-2} \left(\frac{1\ {\rm GeV}}{M_I}\right) , \tag{20}$$

which becomes much smaller than other elements in Eq. (17) for $X_\omega \gg 1$. We should mentioned that the above cancellation in $|\Theta_{eI}|^2$ can be realized for any choice of masses M_2 and M_3. As we will show in Fig. 1, the strong suppression in $|\Theta_{eI}|^2$ is still possible when θ_{13} is close to $\theta_{13}^{\rm cr}$. On the other hand, when $\theta_{13} = 0$, $|\Theta_{eI}|^2$ receives no strong suppression described above, but it satisfies the relation

$$\frac{|\Theta_{eI}|^2}{|\Theta_{\mu I}|^2} \simeq \frac{|\Theta_{eI}|^2}{|\Theta_{\tau I}|^2} \simeq 2\, r_m \sin^2\theta_{12} \simeq 0.11 . \tag{21}$$

This relation had already been obtained in Ref. [26].

In Fig. 1 we show the mixing elements $|\Theta_{\alpha 2}|^2$ in terms of X_ω when $M_2 = 120$ MeV. First, we observe that $|\Theta_{\mu 2}|^2$ and $|\Theta_{\tau 2}|^2$ scales as X_ω^2 for $X_\omega \gg 1$, and they can take much larger values than the naive result in Eq. (12). This behavior does not change much as long as θ_{13} lies in the experimentally allowed region. Second, when $\sin^2\theta_{13} = 0$, $|\Theta_{e2}|^2$ behaves similar to $|\Theta_{\mu 2}|^2$ and $|\Theta_{\tau 2}|^2$ for $X_\omega \gg 1$, but is smaller by one order of magnitude as shown in Eq. (21). Finally, it is clearly seen that $|\Theta_{e2}|^2$ can be suppressed by many orders of magnitude for $X_\omega \gg 1$ when θ_{13} becomes close to its critical value with a suitable parameter choice. Moreover, if $\theta_{13} = \theta_{13}^{\rm cr}$, we

[#3] When we use the data at 2σ level, $\sin^2\theta_{13}^{\rm cr} = 0.046$–$0.065$, which exceeds the 2σ bound $\sin^2\theta_{13} < 0.039$.

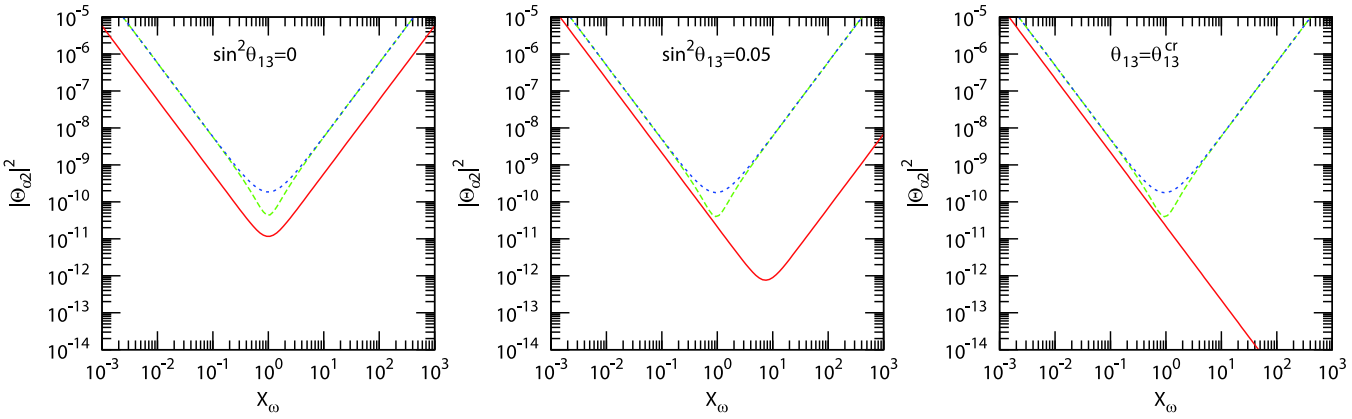

Figure 1: Mixing elements $|\Theta_{\alpha 2}|^2$ in the normal hierarchy in terms of X_ω. We take $\sin^2\theta_{13} = 0$ (left), 0.05 (center) and $\sin^2\theta_{13}^{\rm cr}$ (right), respectively. The red solid, green dashed and blue dotted lines correspond to $|\Theta_{e2}|^2$, $|\Theta_{\mu 2}|^2$ and $|\Theta_{\tau 2}|^2$, respectively. Here we take $M_2 = 120$ MeV, ${\rm Re}\omega = \pi/4$, $\delta = \pi/2$, $\eta = \pi$, and $\xi = +1$.

can see that $|\Theta_{e2}|^2$ is proportional to X_ω^{-2} and it can be extremely suppressed for $X_\omega \gg 1$. The cancellation of $|\Theta_{eI}|^2$ in the NH case is one of the most important observation in this analysis and we will discuss its impacts on the experimental signatures of N_2 and N_3 later.

On the other hand, when $X_\omega \ll 1$ (*i.e.*, ${\rm Im}\omega \ll -1$), the leading order contribution is proportional to X_ω^{-2} and their expressions are given by Eqs.(14), (15) and (16) by replacing X_ω^2 by X_ω^{-2} and ξ by $-\xi$ due to the general property (iv). Therefore, the above arguments with the opposite sign of ξ exactly hold and we will discard this case in the followings.

Next, we turn to discuss the IH case when $X_\omega \gg 1$. In this case, the leading term of the mixing element of electron type is found as

$$|\Theta_{eI}|^2\big|_{X_\omega^2} = \frac{X_\omega^2\, m_2}{4M_I}\cos^2\theta_{12}\cos^2\theta_{13}\left[\tan^2\theta_{12} - 2\xi\sin\eta\sqrt{\frac{m_1}{m_2}}\tan\theta_{12} + \frac{m_1}{m_2}\right], \qquad (22)$$

and the expressions for $|\Theta_{\mu I}|^2$ and $|\Theta_{\tau I}|^2$ are so long and they are collected in App. A. It is interesting to note that the X_ω^2 term as well as the X_ω^0 term in $|\Theta_{eI}|^2$ vanishes when

$$\xi\sin\eta = +1 \quad \text{and} \quad \tan\theta_{12} = \tan\theta_{12}^{\rm cr} = \sqrt{\frac{m_1}{m_2}} = (1 + r_m^2)^{-1/4}, \qquad (23)$$

and then $\theta_{12}^{\rm cr}$ is close to the maximal angle $\pi/4$. Unfortunately, it is far beyond the current data of 3σ range, and the cancellation in $|\Theta_{eI}|^2$ cannot be realized in the IH case, which is different from the NH case.[#4] This point gives significant effects on the discussions given in the following sections.

However, "$\xi\sin\eta$" plays a crucial role to determine the mixing element $|\Theta_{eI}|$. To see this point, let us take $\theta_{23} = \pi/4$ and $\theta_{13} = 0$ for simplicity. In this case, the mixing elements are

[#4] When $\xi\sin\eta = -1$, $\tan\theta_{12} = \sqrt{m_2/m_1}$, and $\sin\theta_{13} = 0$, the X_ω^2 terms in both $|\Theta_{\mu I}|^2$ and $|\Theta_{\tau I}|^2$ vanish at the same time. However, the required value of θ_{12} is not allowed by the current data.

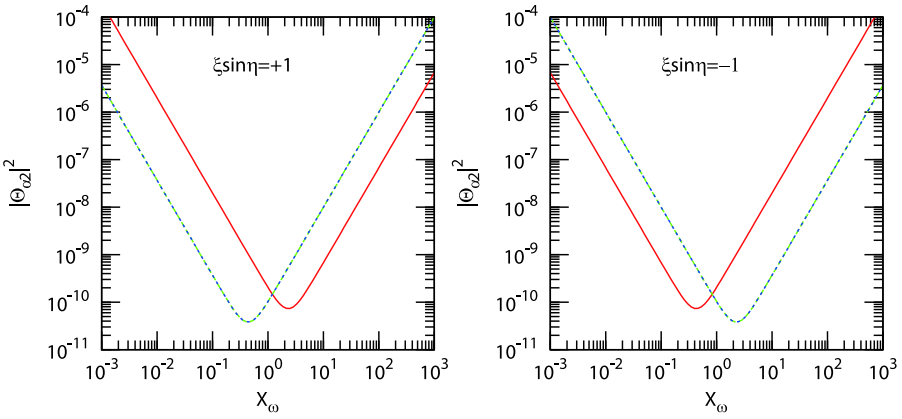

Figure 2: Mixing elements $|\Theta_{\alpha 2}|^2$ in the inverted hierarchy in terms of X_ω. We take $\sin\eta = \pi/2$ (left) and $3\pi/2$ (right), respectively. The red solid, green dashed and blue dotted lines correspond to $|\Theta_{e2}|^2$, $|\Theta_{\mu 2}|^2$ and $|\Theta_{\tau 2}|^2$, respectively. Here we take $M_2 = 120$ MeV, $\mathrm{Re}\omega = \pi/4$, $\delta = \pi/2$, $\theta_{13} = 0$, and $\xi = +1$.

given by

$$|\Theta_{eI}|^2\big|_{X_\omega^2} \simeq \frac{X_\omega^2 m_{\rm atm}}{4M_I}(1 - \xi \sin\eta \sin 2\theta_{12})\,, \tag{24}$$

$$|\Theta_{\mu I}|^2\big|_{X_\omega^2} \simeq |\Theta_{\tau I}|^2\big|_{X_\omega^2} \simeq \frac{X_\omega^2 m_{\rm atm}}{8M_I}(1 + \xi \sin\eta \sin 2\theta_{12})\,, \tag{25}$$

which gives the relation [26]

$$\frac{|\Theta_{eI}|^2}{|\Theta_{\mu I}|^2} \simeq \frac{|\Theta_{eI}|^2}{|\Theta_{\tau I}|^2} \simeq 2\,\frac{1 - \xi \sin\eta \sin 2\theta_{12}}{1 + \xi \sin\eta \sin 2\theta_{12}} = \begin{cases} 0.071 & \text{for } \xi \sin\eta = +1 \\ 56 & \text{for } \xi \sin\eta = -1 \end{cases}\,. \tag{26}$$

Therefore, the mixing element of electron type can be smaller or larger than others depending on the choice of "$\xi \sin\eta$". This property is represented in Fig. 2. It is seen that $|\Theta_{\mu I}|^2$ and $|\Theta_{\tau I}|^2$ are almost the same, but $|\Theta_{eI}|^2$ can be different from others.

Before closing this section, we would like to stress again that the above results of the hierarchy between the mixing elements $\Theta_{\alpha I}$ are independent on the masses of sterile neutrinos. Therefore, they can be applied to the general seesaw models with two right-handed neutrinos.

4 Neutrinoless Double Beta Decay

The neutrinoless double beta ($0\nu 2\beta$) decay is one important phenomenon in which the mixing of active and sterile neutrinos, $U_{\alpha i}$ and $\Theta_{\alpha I}$, plays a crucial role. The $0\nu 2\beta$ decay in the νMSM had already been investigated in Ref. [40], in which the contributions from active neutrinos and dark-matter sterile neutrino N_1 are estimated and those from $N_{2,3}$ are neglected since their masses are assumed to be so heavy that they decouple from the considering decay processes. Further, it had been discussed in Ref. [41] that the $0\nu 2\beta$ decay gives the stringent constraint on

the mixing element Θ_{eI} especially when their masses are around 100 MeV. Following to these analyses, we would like to reconsider this issue in this section. In particular, we shall take into account the contributions from $N_{2,3}$ by considering a wider range of their masses, and also the mixing elements $\Theta_{\alpha 2,3}$ discussed in the previous section. We will then show that the constraints from the $0\nu 2\beta$ decay are negligible in the νMSM.

The rate of the $0\nu 2\beta$ decay is characterized by the effective neutrino mass $m_{\rm eff}$ (see, *e.g.*, Ref. [48]). In the νMSM it is given by

$$m_{\rm eff} = m^{\nu}_{\rm eff} + \sum_{I=1,2,3} M_I \, \Theta^2_{eI} \, f_\beta(M_I) \,, \tag{27}$$

where the first term $m^{\nu}_{\rm eff}$ denotes the contribution from active neutrinos

$$m^{\nu}_{\rm eff} = \sum_{i=1,2,3} m_i U^2_{ei} \,. \tag{28}$$

The second term in Eq. (27) denotes the contribution from sterile neutrinos in which we have introduced the function f_β to represent the suppression of the nuclear matrix element from neutrinos with masses heavier than about 100 MeV [49, 50]. In this analysis, for simplicity, we shall assume $f_\beta(M_I) = 1$ for $M_I \leq \Lambda_\beta$ and $f_\beta(M_I) = (\Lambda_\beta/M_I)^2$ for $M_I > \Lambda_\beta$ where the typical energy scale in the matrix element is taken as $\Lambda_\beta = 100$ MeV. The more precise treatment of the function f_β at $M_I \simeq \Lambda_\beta$ does not alter our final conclusions.

First, we consider the case when all the sterile neutrinos in the νMSM are lighter than Λ_β. As for the dark-matter sterile neutrino N_1, its mass is indeed smaller than Λ_β. On the other hand, the masses of N_2 and N_3 can be smaller or larger than Λ_β. Here we consider the former case and the latter case will be discussed separately below. In this case the effective neutrino mass exactly vanishes. This is because

$$m_{\rm eff} = \sum_{i=1,2,3} m_i \, U^2_{ei} + \sum_{I=1,2,3} M_I \, \Theta^2_{eI} = [\, \hat{U} \, \hat{M}^{\rm diag}_{\nu} \, \hat{U}^T \,]_{ee} = [\hat{M}_\nu]_{ee} = 0 \,. \tag{29}$$

This cancellation has been recently observed in Ref. [50] by using the general seesaw model. Thus, the νMSM with $M_{1,2,3} < \Lambda_\beta$ predicts zero event in the $0\nu 2\beta$ decay, which means that the current experimental limits on $m_{\rm eff}$ give no constraint on the model.

On the other hand, $N_{2,3}$ can be heavier than Λ_β in the νMSM. In this case, the prediction of $m_{\rm eff}$ is modified. We consider the case when N_1 is resonantly produced via thermal scatterings in the presence of the lepton asymmetries as mentioned in Sec. 2. In this case, as already pointed out in Ref. [40], the contribution from dark-matter sterile neutrino N_1, denoted by $m^{N_1}_{\rm eff}$, is very small. The correct abundance of dark matter can be obtained when $M_1 = 4$–50 keV and $|F_{\alpha 1}| \simeq 5 \times 10^{-15}$–$4 \times 10^{-13}$ [27]. Since $M_1 < \Lambda_\beta$, we find

$$|m^{N_1}_{\rm eff}| = M_1 \, |\Theta^2_{e1}| = \frac{|F^2_{e1}| \, \langle \Phi \rangle^2}{M_1} = \mathcal{O}(10^{-11}\text{–}10^{-6}) \ \text{eV} \,, \tag{30}$$

which is so small to be negligible in most cases, but we will point out its importance.

Let us turn to consider the contribution from N_2 and N_3. These sterile neutrinos are quasi-degenerate in order for the successful baryogenesis [34, 6, 36, 37]. We then write the masses as $M_3 = M_N + \Delta M/2$ and $M_2 = M_N - \Delta M/2$ with $\Delta M \ll M_N$, and divide $m_{\rm eff}$ from $N_{2,3}$ into two parts

$$m_{\rm eff}^{N_{2,3}} = \sum_{I=2,3} M_I \Theta_{eI}^2 f_\beta(M_I) = \bar{m}_{\rm eff}^{N_{2,3}} + \delta m_{\rm eff}^{N_{2,3}} \,, \tag{31}$$

where

$$\bar{m}_{\rm eff}^{N_{2,3}} = f_\beta(M_N) \sum_{I=2,3} M_I \Theta_{eI}^2 \,, \tag{32}$$

$$\delta m_{\rm eff}^{N_{2,3}} = \sum_{I=2,3} \left[f_\beta(M_I) - f_\beta(M_N) \right] \, M_I \Theta_{eI}^2 \,. \tag{33}$$

Notice that the second part $\delta m_{\rm eff}^{N_{2,3}}$ vanishes when $\Delta M = 0$, and more interestingly, that the first term can be written as

$$\bar{m}_{\rm eff}^{N_{2,3}} = -f_\beta(M_N)\, m_{\rm eff}^\nu \,. \tag{34}$$

Therefore, the effective neutrino mass in the νMSM when $M_{2,3} > \Lambda_\beta$ is written as

$$m_{\rm eff} = \left[1 - f_\beta(M_N) \right] m_{\rm eff}^\nu + m_{\rm eff}^{N_1} + \delta m_{\rm eff}^{N_{2,3}} \,. \tag{35}$$

It is then found that when $M_N \gg \Lambda_\beta$ (and hence $f_\beta(M_{2,3}) \ll 1$)

$$m_{\rm eff} \simeq m_{\rm eff}^\nu + m_{\rm eff}^{N_1} \,, \tag{36}$$

which shows the sizable contributions come only from active neutrinos and dark-matter sterile neutrino [40]. On the other hand, N_2 and N_3 give a significant effect on $m_{\rm eff}$ especially when they are quasi-degenerate and $M_N \simeq \Lambda_\beta$, namely, they induce the destructive contribution to $m_{\rm eff}$ given in Eq. (27). Thus, $|m_{\rm eff}|$ in the νMSM can be much smaller than $|m_{\rm eff}^\nu|$ when $M_N \simeq \Lambda_\beta$. This point is illustrated in Fig. 3, where we show the allowed region of $|m_{\rm eff}|$ in terms of M_N by varying Reω, δ and η in the range $[0, 2\pi]$, Imω in the range $[0, 7]$, and the parameters of active neutrinos within the experimental 3σ range.

Next, we turn to see how $m_{\rm eff}$ depends on masses, mixing angles and CP violating phases of active neutrinos. In the NH case, the contribution from active neutrinos is (*e.g.*, see [51])

$$m_{\rm eff}^\nu = e^{-2i\delta} \left(\sin^2\theta_{13}\, m_3 + e^{2i(\delta+\eta)} \, \cos^2\theta_{13} \, \sin^2\theta_{12}\, m_2 \right) \,. \tag{37}$$

Notice that $m_1 = 0$ in the limit of $F_{\alpha 1} \to 0$. We also find that

$$\begin{aligned} \delta m_{\rm eff}^{N_{2,3}} &= \frac{\Delta M}{2} f'_\beta(M_N) \left[M_3\, \Theta_{e3}^2 - M_2\, \Theta_{e2}^2 \right] \\ &= e^{-2i\delta} \frac{\Delta M\, \Lambda_\beta^2}{2 M_N^3} \Big[X_\omega^2\, e^{-2i{\rm Re}\omega} \left(\sqrt{m_3}\xi \sin\theta_{13} - i e^{i(\delta+\eta)} \sqrt{m_2} \cos\theta_{13} \sin\theta_{12} \right)^2 \\ &\qquad + X_\omega^{-2}\, e^{+2i{\rm Re}\omega} \left(\sqrt{m_3}\xi \sin\theta_{13} + i e^{i(\delta+\eta)} \sqrt{m_2} \cos\theta_{13} \sin\theta_{12} \right)^2 \Big] \,, \end{aligned} \tag{38}$$

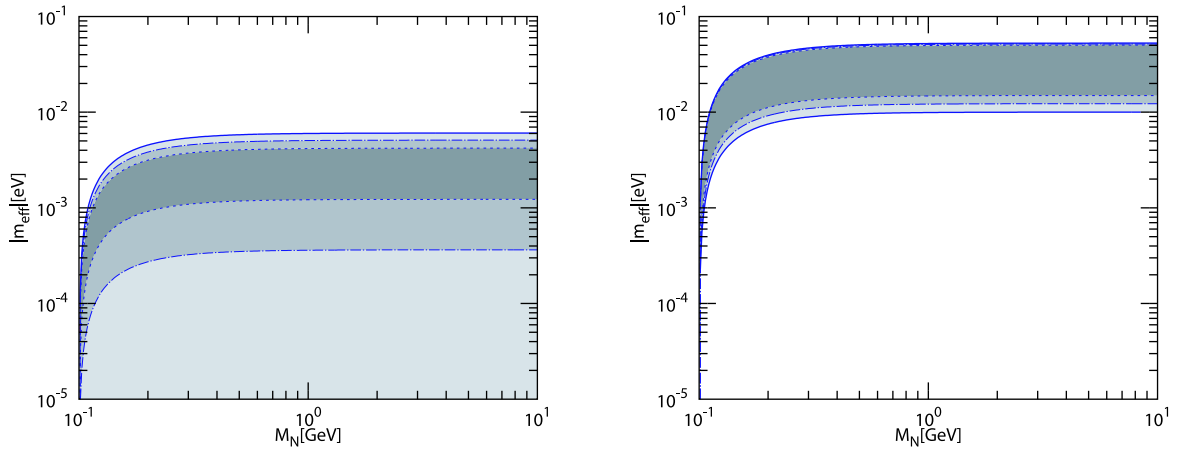

Figure 3: Allowed regions for $|m_{\rm eff}|$ as a function of the mass of sterile neutrino M_N, for NH (left) and IH (right) cases, respectively. The light gray region with solid lines, gray region with dot-dashed lines, and dark gray region with dotted lines correspond to regions allowed by the observational data for active neutrinos at the 3σ, 2σ and 1σ level, respectively. Here we take $\Delta M/M_N = 5 \times 10^{-8}$.

where we have neglected the higher order terms of ΔM.

It should be noted that $m^{\nu}_{\rm eff}$ and also the X^2_ω term in $\delta m^{N_{2,3}}_{\rm eff}$ vanish, if $\cos 2(\delta + \eta) = -1$ and $\tan^2\theta_{13} = r_m \sin^2\theta_{12}$. Interestingly, the required conditions are the same as (18) and (19), *i.e.*, those for the cancellation in $|\Theta_{eI}|^2$. In this case, $\delta m^{N_{2,3}}_{\rm eff}$ becomes suppressed for a large X_ω together with a small mass difference of $N_{2,3}$. As a result, the dark-matter sterile neutrino gives the dominant contribution to the effective mass in the $0\nu2\beta$ decay $|m_{\rm eff}| \simeq |m^{N_1}_{\rm eff}|$, which is very small as shown in Eq. (30). This is the reason why the 3σ lower bound on $|m_{\rm eff}|$ is beyond the region of the plot.

When the conditions (18) and (19) are not satisfied, we find for large X_ω

$$|\delta m^{N_{2,3}}_{\rm eff}| \simeq 1.5 \times 10^{-12}\ {\rm eV} \left(\frac{\Delta M/M_N}{5\times 10^{-8}}\right) \left(\frac{1\ {\rm GeV}}{M_N}\right)^2 X^2_\omega\,, \tag{39}$$

by using the central values of parameters of active neutrinos and $\delta + \eta = \pi/2$.[#5] This shows that we may neglect $\delta m^{N_{2,3}}_{\rm eff}$ as long as ΔM is sufficiently small. Note that X_ω cannot be so large due to the experimental upper bounds on $\Theta_{\alpha I}$, which will be investigated in the next section. In this case, the effective neutrino mass becomes

$$m_{\rm eff} \simeq [1 - f_\beta(M_N)]\, m^{\nu}_{\rm eff} + m^{N_1}_{\rm eff}\,. \tag{40}$$

We then understand the 3σ upper bound on $|m_{\rm eff}|$ in Fig. 3 as $[1 - f_\beta(M_N)]\, m^{\nu}_{\rm eff}\big|_{\rm MAX}$, which becomes suppressed when M_N is close to Λ_β.

In the IH case, we obtain

$$m^{\nu}_{\rm eff} = \cos^2\theta_{13} \left(\cos^2\theta_{12}\, m_1 + e^{2i\eta} \sin^2\theta_{12}\, m_2\right)\,, \tag{41}$$

[#5] Here the maximal value of $|\delta m^{N_{2,3}}_{\rm eff}|$ is shown. When $\delta + \eta = 3\pi/2$, it takes the minimal value and the prefactor becomes 1.8×10^{-13}.

and

$$\begin{aligned}\delta m_{\rm eff}^{N_{2,3}} &= \frac{\Delta M}{2} f'_\beta(M_N)\left[M_3\,\Theta_{e3}^2 - M_2\,\Theta_{e2}^2\right] \\ &= -\frac{\Delta M \Lambda_\beta^2}{2M_N^3}\cos^2\theta_{13}\left[X_\omega^2\, e^{-2i{\rm Re}\omega}\left(\sqrt{m_1}\xi\cos\theta_{12} + i\, e^{i\eta}\sqrt{m_2}\sin\theta_{12}\right)^2\right. \\ &\qquad \left. + X_\omega^{-2}\, e^{+2i{\rm Re}\omega}\left(\sqrt{m_1}\xi\cos\theta_{12} - i\, e^{i\eta}\sqrt{m_2}\sin\theta_{12}\right)^2\right]. \end{aligned} \tag{42}$$

Then, as in the NH case, $m_{\rm eff}^\nu$ as well as the X_ω^2 term in $\delta m_{\rm eff}^{N_{2,3}}$ vanish, when $\xi\sin\eta = +1$ and $\tan^2\theta_{12} = m_1/m_2$. The required conditions are the same as those of the cancellation in $|\Theta_{eI}|$, and they are not satisfied the present experimental data on the masses and mixing angles of active neutrinos. This is the reason why $|m_{\rm eff}|$ in the IH case receives the stringent lower bound as shown in Fig. 3, and $m_{\rm eff}^{N_1}$ becomes negligible. Further, compared with other terms, $\delta m_{\rm eff}^{N_{2,3}}$ can be neglected for a small mass difference of $N_{2,3}$. This is because

$$|\delta m_{\rm eff}^{N_{2,3}}| \simeq 2.3\times 10^{-11}\ {\rm eV}\left(\frac{\Delta M/M_N}{5\times 10^{-8}}\right)\left(\frac{1\ {\rm GeV}}{M_N}\right)^3 X_\omega^2\,, \tag{43}$$

when we take $\eta = 3\pi/2$. [#6] Therefore, we obtain in the IH case

$$m_{\rm eff} \simeq \left[1 - f_\beta(M_N)\right] m_{\rm eff}^\nu\,. \tag{44}$$

In summary, we have shown that the effective neutrino mass in the $0\nu2\beta$ decay is given by the contribution from active neutrinos $m_{\rm eff}^\nu$ (together with a very small $m_{\rm eff}^{N_1}$) for $M_{2,3} \gg \Lambda_\beta$. On the other hand, when $M_{2,3} \sim \Lambda_\beta$, sterile neutrinos N_2 and N_3 give the destructive contribution and then $m_{\rm eff}$ becomes much smaller than that from active neutrinos. Especially, $m_{\rm eff}$ vanishes when all the sterile neutrinos are lighter than Λ_β. Therefore, the νMSM receives no stringent constraint on the mixing elements $\Theta_{\alpha I}$ from the $0\nu2\beta$ decay pointed out in Ref. [41].

5 Search for light sterile neutrinos

In this section we shall discuss the experimental search of sterile neutrinos $N_{2,3}$. In particular, we restrict ourselves here to the case when the masses are smaller than the pion mass. This is simply because we would like to discuss the production of $N_{2,3}$ in the decays of π^+ and K^+. In addition, although such light sterile neutrinos have a long lifetime and may decay after the big bang nucleosynthesis (BBN) starts as we will show below, it can be avoided the stringent constraint from the BBN [52] on the hadronic decays of $N_{2,3}$. In this section, we shall explore in detail the impacts of the results in Sec. 3 on the direct searches of $N_{2,3}$ in the π^+ and K^+ decays.

[#6] Here the maximal value of $|\delta m_{\rm eff}^{N_{2,3}}|$ is shown. When $\eta = \pi/2$, it takes the minimal value and the prefactor becomes 8.0×10^{-13}.

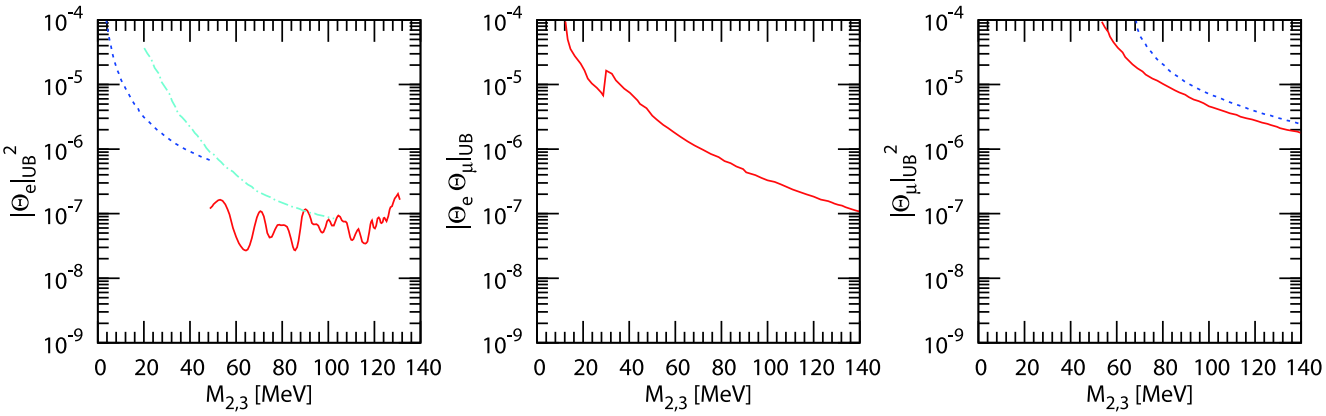

Figure 4: Upper bounds on $|\Theta_{eI}|^2$ (left), $|\Theta_{eI}\Theta_{\mu I}|$ (center) and $|\Theta_{\mu I}|^2$ (right) from direct searches of sterile neutrino. In the left panel the red sold line is from [54], the blue dotted line is from [55], and the cyan dot-dashed line is from [59]. In the center panel the red solid line is from [59]. In the right panel the red solid line is from [56], and the blue dashed line is from [57].

There have been so far various experiments of the direct search for sterile neutrino which give the upper bounds on the mixing elements $\Theta_{\alpha I}$. In the considering mass region, the signal of sterile neutrino can be investigated by the peak search [53] in the energy spectrum of charged leptons from meson decays [54]-[57], and also by finding charged leptons from the decays of sterile neutrino inside the detector [58]-[60]. See, for example, Refs. [61, 38, 62]. The upper bounds on the mixing elements are summarized in Fig. 4. Notice that the upper bound on $|\Theta_{\tau I}|$ [60] is weaker than that on $|\Theta_{\mu I}|$, and then it plays no significant role for our conclusion. It can be seen that the bound on $|\Theta_{eI}|$ is severer than $|\Theta_{\mu I}|$ by orders of magnitude.

The mixing elements of $N_{2,3}$ scale as $|\Theta_{\alpha I}| \propto X_\omega$ for $X_\omega \gg 1$, as described in Sec. 3. Thus, the experimental upper bounds on $|\Theta_{\alpha I}|$ can be translated into the upper bound on X_ω. Such a bound is the basis of finding the shortest lifetimes of N_2 and N_3 and also the largest production rates in the decays of π^+ and K^+. Let us first discuss the case when $M_N = 120$ MeV. In this case, the experimental bounds are $|\Theta_{eI}|^2_{\rm UB} = 6.0 \times 10^{-8}$, $|\Theta_{eI}\Theta_{\mu I}|_{\rm UB} = 1.8 \times 10^{-7}$, and $|\Theta_{\mu I}|^2_{\rm UB} = 2.8 \times 10^{-6}$.

In the NH case, we show in Fig. 5 the upper bounds on X_ω in terms of $\sin^2\theta_{13}$ since the element Θ_{eI} is crucially dependent on this mixing angle. When there is no cancellation in Θ_{eI} (see the left panel of Fig. 5), the experimental bound on $|\Theta_{eI}|^2$ determines the upper bound on X_ω in most cases. Note that, when θ_{13} is close to zero, $|\Theta_{eI}|^2$ is smaller than $|\Theta_{\mu I}|^2$ by one order of magnitude as shown in Eq. (21) and then $|\Theta_{eI}\Theta_{\mu I}|_{\rm UB}$ puts the upper bound on X_ω.

On the other hand, as shown in the right panel of Fig. 5, the situation is drastically changed when the cancellation in Θ_{eI} can happen as shown in Eqs. (18) and (19). In this case, the experimental bounds on $|\Theta_{eI}|^2$ and also $|\Theta_{eI}\Theta_{\mu I}|$ play no significant roles, but that on $|\Theta_{\mu I}|^2$ determines the upper bound on X_ω. Since the present limit $|\Theta_{\mu I}|^2_{\rm UB}$ is weaker than others, the allowed region of X_ω becomes wider. Furthermore, we find that the CP violating phases

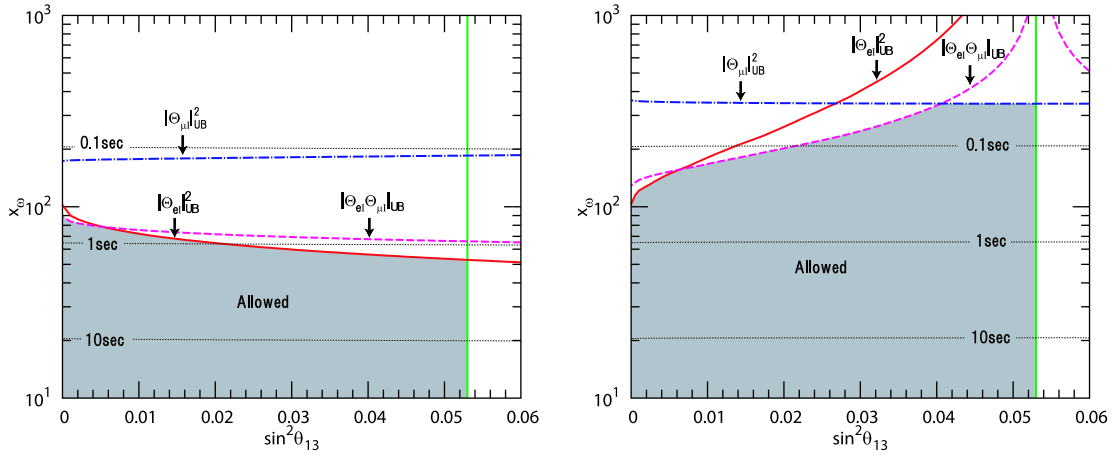

Figure 5: Allowed region in the $\sin^2\theta_{13}$-X_ω plane for the NH case by taking $\delta = 0$ and $\eta = \frac{\pi}{2}$ (left) and $\delta = 0$ and $\eta = \frac{3\pi}{2}$ (right). The red solid, the magenta dashed, and the blue dot-dashed lines are the upper bounds on X_ω from the experimental limits on $|\Theta_{eI}|^2$, $|\Theta_{eI}\Theta_{\mu I}|$, and $|\Theta_{\mu I}|^2$ respectively. The green line is the 3σ limit on $\sin^2\theta_{13}$. The black dotted lines show lifetimes of sterile neutrino. We take $M_3 = 120$MeV, $\Delta M^2/M_3^2 = 10^{-8}$, Re$\omega = \frac{\pi}{4}$, and $\xi = +1$.

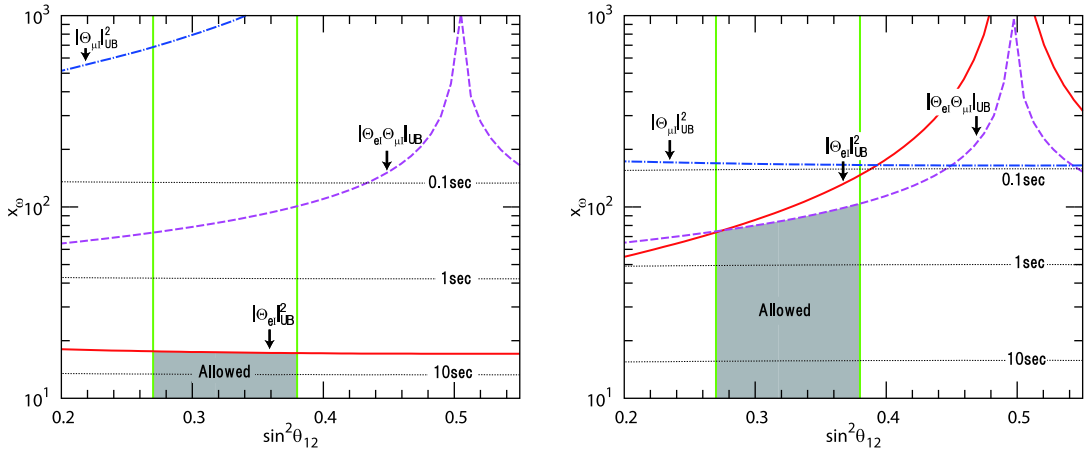

Figure 6: Allowed region in the $\sin^2\theta_{12}$-X_ω plane for the IH case by taking $\delta = \frac{\pi}{2}$ and $\eta = \frac{3\pi}{2}$ (left) and $\delta = \frac{\pi}{2}$ and $\eta = \frac{\pi}{2}$ (right). The red solid, the magenta dashed, and the blue dot-dashed lines are the upper bounds on X_ω from the experimental limits on $|\Theta_{eI}|^2$, $|\Theta_{eI}\Theta_{\mu I}|$, and $|\Theta_{\mu I}|^2$ respectively. The green lines shows the 3σ range of $\sin^2\theta_{12}$. The black dotted lines show lifetimes of sterile neutrino. We take $M_3 = 120$MeV, $\Delta M^2/M_3^2 = 10^{-8}$, $\theta_{13} = 0$, Re$\omega = \frac{\pi}{4}$ and $\xi = +1$.

change importantly the prediction of $|\Theta_{\mu I}|$ even when the condition (18) is satisfied. This is because, as found from Eq. (52) in App. A, the negative $\xi \sin\eta$ decreases $|\Theta_{\mu I}|$. For instance, if we compare two sets of the CP phases, ($\delta = \pi$, $\eta = \pi/2$) and ($\delta = 0$, $\eta = 3\pi/2$), satisfying the condition (18) with $\xi = +1$, the latter case gives the suppressed $|\Theta_{\mu I}|$ for $X_\omega \gg 1$ and X_ω can be about 350 as shown in Fig. 5.[#7]

[#7]Here we have used the central values of parameters of active neutrinos. When we vary them in the 3σ range, X_ω can be large as about 550 as shown in Fig. 7

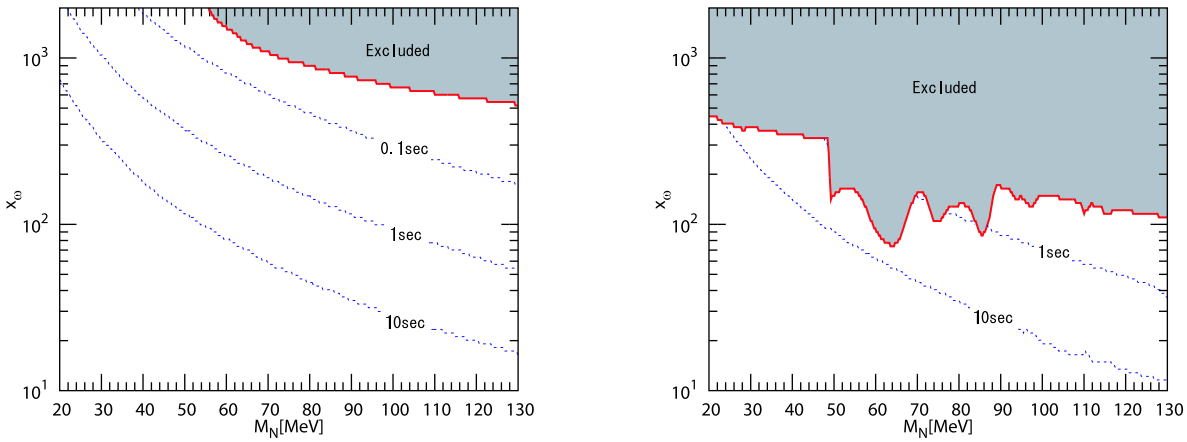

Figure 7: Allowed region in the M_N-X_ω plane for the NH (left) and IH (right) cases. The gray region is excluded by experiments for direct search of sterile neutrinos. The dotted lines show the lower bounds on X_ω for given lifetime of sterile neutrino. We use the observational data for active neutrinos at the 3σ level.

In the IH case, the mixing angle θ_{12} is an important parameter to determine $\Theta_{\alpha I}$ and then we represent in Fig. 6 the upper bounds on X_ω in terms of $\sin^2\theta_{12}$. Since the cancellation in Θ_{eI} cannot be realized in the IH case, the experimental bounds on $|\Theta_{eI}|^2$ and $|\Theta_{eI}\Theta_{\mu I}|$ place the upper bound on X_ω. As explained in Eq. (26), the choice of "$\xi \sin\eta$" is significant to determine the ratio $|\Theta_{eI}|/|\Theta_{\mu I}|$. When $\xi\sin\eta = -1$ (*e.g.*, $\xi = +1$ and $\eta = 3\pi/2$), $|\Theta_{eI}|$ becomes larger than $|\Theta_{\mu I}|$. In this case, the upper bound on X_ω becomes smaller due to the stringent experimental bound on $|\Theta_{eI}|$ (see the left panel of Fig. 6). Inversely, when $\xi\sin\eta = +1$ (*e.g.*, $\xi = +1$ and $\eta = \pi/2$), $|\Theta_{eI}|$ becomes smaller than $|\Theta_{\mu I}|$. Then, the upper bound on X_ω becomes relaxed and X_ω can be large as about 100 (see the right panel of Fig. 6).

We then find numerically the upper bound on X_ω for a given $M_{2,3}$ by varying Reω, δ and η in the range $[0, 2\pi]$ and also by varying the parameters of active neutrinos within the experimental 3σ range. The obtained results are shown in Fig. 7. In the NH case, the upper bound becomes weaker for lighter M_N. Especially, no sensible bound is available for $M_N \lesssim 55$ MeV. This is because the cancellation in Θ_{eI} is possible and also because there is no stringent experimental bound on $|\Theta_{\mu I}|^2$ for such mass region. It is quite interesting to note that X_ω at $\mathcal{O}(10^2$-$10^3)$ is experimentally allowed for $M_N \sim 100$ MeV. In the IH case, on the other hand, we can see that the bound on X_ω is severer than that in the NH case. This is because there is no cancellation in Θ_{eI} and X_ω always receives the stringent experimental bounds on $|\Theta_{eI}|^2$ and/or $|\Theta_{eI}\Theta_{\mu I}|$ as explained above.

The upper bound of X_ω allows us to estimate the possible range of the lifetimes of N_2 and N_3. The lifetime is a key parameter from the following two reasons. One reason is concerned with the search for N_2 and N_3. In the test of sterile neutrino by finding charged leptons from its decay inside the detector, the lifetime determines the decay length and also the detection rate. The other comes from cosmology. The light sterile neutrinos under consideration can be long-lived particles and their decays would spoil the success of the standard cosmology, especially

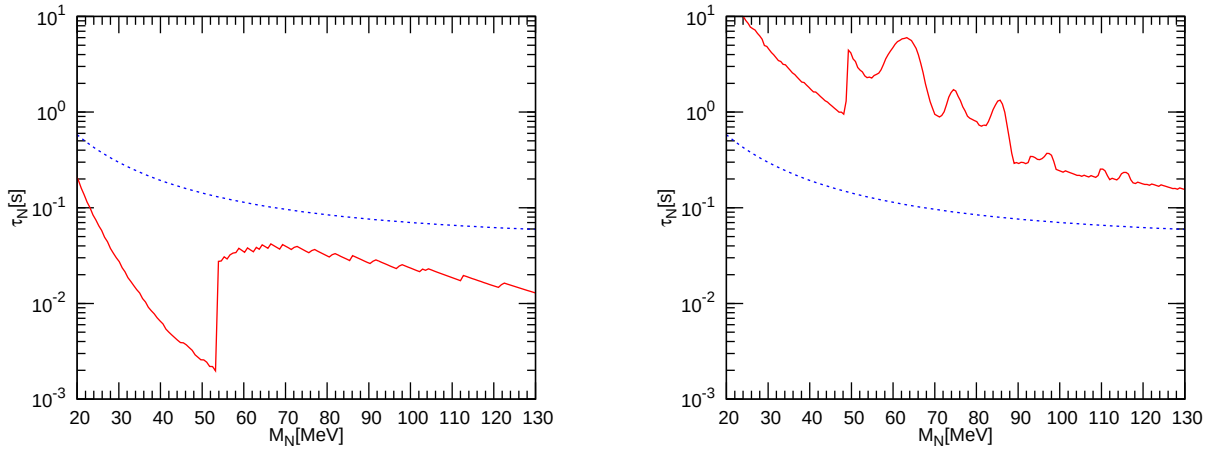

Figure 8: Lower bounds on lifetime of sterile neutrino in terms of M_N is shown by the red solid lines for the NH (left) and IH (right) cases. We use the upper bound on the mixing elements for sterile neutrinos, $|\Theta_{eI}|^2_{\rm UB}$, $|\Theta_{\mu I}|^2_{\rm UB}$, $|\Theta_{eI}\Theta_{\mu I}|_{\rm UB}$ and the observational data for active neutrinos at the 3σ level. The BBN upper bounds on lifetime in Eq. (46) are also shown by the blue dotted lines.

the prediction of light elements of BBN. The lifetime is then restricted by various cosmological constraints. We shall discuss this issue later.

In the considering mass region, $N_{2,3}$ decay in to $\nu_i\nu_j\overline{\nu}_j$ or $\nu_i\ell^-_\alpha\ell^+_\beta$ $(\ell_{\alpha,\beta} = e, \mu)$ and their CP conjugate states. The lifetime, which is determined from the mixing elements $\Theta_{\alpha I}$ and the mass of sterile neutrino, can be estimated by using the partial decay rates presented in Refs. [64, 43, 38]. Before dealing with the actual model, we consider the toy model described in Eq. (12). In this case, since the dominant channel is the decay into three active neutrinos, the lifetime is estimated as

$$\tau_N \simeq \frac{192\pi^3}{G_F^2|\Theta|^2 M_N^5} = 6\times 10^3\,\text{sec}\left(\frac{m_{\rm atm}}{m_\nu}\right)\left(\frac{100\ \text{MeV}}{M_N}\right)^4 . \tag{45}$$

Therefore, sterile neutrino decays after BBN starts, which might lead to cosmological difficulty. In the νMSM, however, this is not always the case and the much shorter lifetime can be achieved, because the lifetime scales as $\tau_{N_{2,3}} \propto X_\omega^{-2}$ for $X_\omega \gg 1$. Thus, a sufficiently large X_ω makes $N_{2,3}$ cosmologically harmless.

We find, as general properties, that the lifetimes of N_2 and N_3 are almost the same, and also that the lifetime in the IH case is slightly shorter than the NH case for a given X_ω. We then show the contour lines of lifetime of $N_{2,3}$ in the parameter regions discussed previously (see Figs. 5, 6 and 7). It is seen that the lifetime can vary orders of magnitude depending on the choice of X_ω. Since we have obtained the upper bound on X_ω to be consistent with the search experiments, we can estimate the lowest value of the lifetime of $N_{2,3}$. The results are shown in Fig. 8 for the NH and IH cases, respectively. In the NH case, the direct searches give no significant constraint on X_ω for $M_N \lesssim 55$ MeV. We then impose $|\Theta_{\alpha I}|^2 < 10^{-2}$ to ensure the validity of the seesaw mechanism. It is found that $\tau_{N_{2,3}}$ of $\mathcal{O}(10^{-2}$–$10^{-1})$ sec is available in the

wide mass range. When the cancellation in Θ_{eI} occurs, the upper bound on X_ω gets larger. As a result, $|\Theta_{\mu I}|$ and $|\Theta_{\tau I}|$ can take the larger values, which leads to the shorter lifetime of $N_{2,3}$ even if $|\Theta_{eI}|$ is very small. In the IH case, on the other hand, the absence of such a cancellation gives the stringent lower bound of $\tau_{N_{2,3}}$ as 10–10^{-1} sec for $M_N = 20$–130 MeV.

It had been pointed out in Ref. [38] that the bound from the BBN places the upper bound on the lifetime of $N_{2,3}$, which results in the admitted window for the parameter space of the model. The decays of sterile neutrinos around the BBN era would alter the abundances of light elements in a desperate way. There are two significant effects by such decays. One effect is that the additional energy carried by sterile neutrinos increases the expansion rate of the universe. The other is the modification of the proton-neutron conversion rate. This is because active neutrinos produced by the decays of $N_{2,3}$ cannot be fully thermalized if the decays occur too late and then the distortion of the distribution functions affects the conversion rate. These two effects would alter the abundance of light elements (^{4}He especially) too much, which leads to the upper bound on $\tau_{N_{2,3}}$. Notice that the stringent constraint from the BBN [52] on the hadronic decays can be avoided in the considering situation.

Such a bound had already been discussed in Refs. [42, 43], in which the authors consider the model with one flavour of active and sterile neutrinos. At present there is no analysis dealing with the realistic situation of the considering model. We shall postpone to study the issue in future publication [63], and just apply the bound on the lifetime given in Ref. [43]. The maximum allowed lifetime $\tau_{\rm BBN}$ is given by

$$\tau_{\rm BBN}/{\rm sec} = t_1 \left(\frac{M_N}{1\ {\rm MeV}}\right)^\beta + t_2\,, \tag{46}$$

where $t_1 = 128.7$, $t_2 = 0.04179$, and $\beta = -1.828$ [43]. (In this analysis we have taken a conservative bound for the mixing with $\nu_{\mu,\tau}$, and see the detail in Ref. [43].) When $M_N = 120$ MeV, we find $\tau_{\rm BBN} = 6.2 \times 10^{-2}$ sec.

In Fig. 8 the BBN bound on the lifetime $\tau_{\rm BBN}$ is also shown in terms of M_N. We can find that, although such a short lifetime cannot be obtained in the IH case, there exits the allowed region in the NH case, which is different from the conclusion in Ref. [38]. This is because of the cancellation in Θ_{eI} we have obtained in Sec. 3, which enlarges the allowed parameter space of the model by relaxing the stringent constraints on $|\Theta_{eI}|$ from direct searches. In this allowed region, we can obtain remarkable predictions of the model parameters. This point is illustrated in Fig. 9 when $M_N = 120$ MeV. First, X_ω should be sufficiently large for $\tau_{N_{2,3}} < \tau_{\rm BBN}$ and $X_\omega \gtrsim 250$ in this case. Second, in order to sufficiently suppress $|\Theta_{eI}|$, the parameters should be very close to those in the conditions (18) and (19). Namely, the mixing angle θ_{13} should be large (close to $\theta_{13}^{\rm cr}$), and the CP violating phases should be $\xi \sin(\delta+\eta) \simeq 1$. Finally, the negative sign of $\xi \sin\eta$ is required to decrease $|\Theta_{\mu I}|$. Therefore, the range of the Chooz angle θ_{13} and the CP phases δ and η is highly restricted. This leads to an important effect on baryogenesis of the model, which will be discussed elsewhere [63].

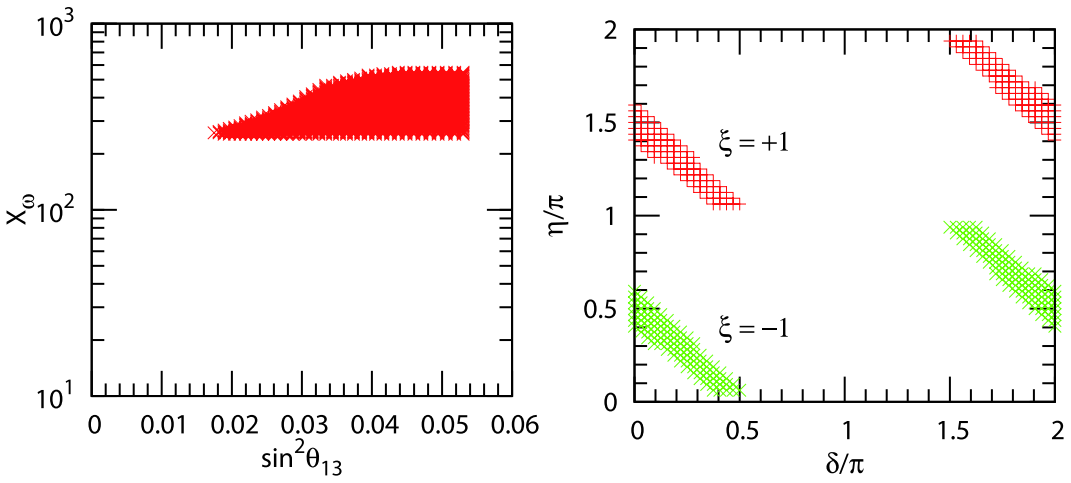

Figure 9: Allowed regions in the $\sin^2\theta_{13}$-X_ω plane (left) and δ-η plane (right) when $\tau_{N_{2,3}} < \tau_{\rm BBN}$ for the NH case. Here we take $M_N = 120$ MeV. In the right-panel red points and green points correspond to the case $\xi = +1$ and $\xi = -1$, respectively.

In the following, however, we shall adopt the upper bound on the lifetime as $\tau_{N_{2,3}} < 1$ sec, in addition to $\tau_{N_{2,3}} < \tau_{\rm BBN}$, as the most conservative case, and consider the both NH and IH cases.

Now, we are at the position to discuss the experimental search of $N_{2,3}$ by the peak searches in the decays $\pi^+ \to e^+ + N_{2,3}$, $K^+ \to e^+ + N_{2,3}$, and $K^+ \to \mu^+ + N_{2,3}$. The branching ratio for the production process is given by [53]

$$\mathrm{BR}(P^+ \to \ell^+ + N_I) = \mathrm{BR}(P^+ \to \ell^+ + \nu_\ell) \times K(m_P, m_\ell, M_I)\,, \tag{47}$$

where $P = \pi, K$ and $\ell = e, \mu$. The function K is

$$K(m_P, m_\ell, M_I) = |\Theta_{\ell I}|^2 \, \frac{\beta_{N_I}}{\beta_\nu} \, \frac{m_P^2(M_I^2 + m_\ell^2) - (M_I^2 - m_\ell^2)^2}{m_P^2 m_\ell^2 - m_\ell^4}\,, \tag{48}$$

where

$$\beta_{N_I}^2 = 1 - 2\frac{M_I^2 + m_\ell^2}{m_P^2} + \frac{(M_I^2 - m_\ell^2)^2}{m_P^4}\,, \qquad \beta_\nu = 1 - \frac{m_\ell^2}{m_P^2}\,. \tag{49}$$

Here we have neglected the masses of active neutrinos. It is then seen that the branching ratios are proportional to the mixing element squared, and hence X_ω^2.

By taking $M_N = 120$ MeV, the allowed regions of the branching ratios are shown in Figs. 10 and 11 for the NH and IH cases, respectively. Here we have imposed the lifetime bound in addition to the experimental bounds on the mixing elements, and the parameters of the Yukawa matrix have been varied as we did before.

In the NH case, it is found that the branching ratios of $\pi^+ \to e^+ + N$ and $K^+ \to e^+ + N$ can be very small even if one imposes the lifetime bound. This is due to the cancellation in $|\Theta_{eI}|$ pointed out in this paper. As explained in Eq. (20), $|\Theta_{eI}|^2$ is proportional to X_ω^{-2} when the

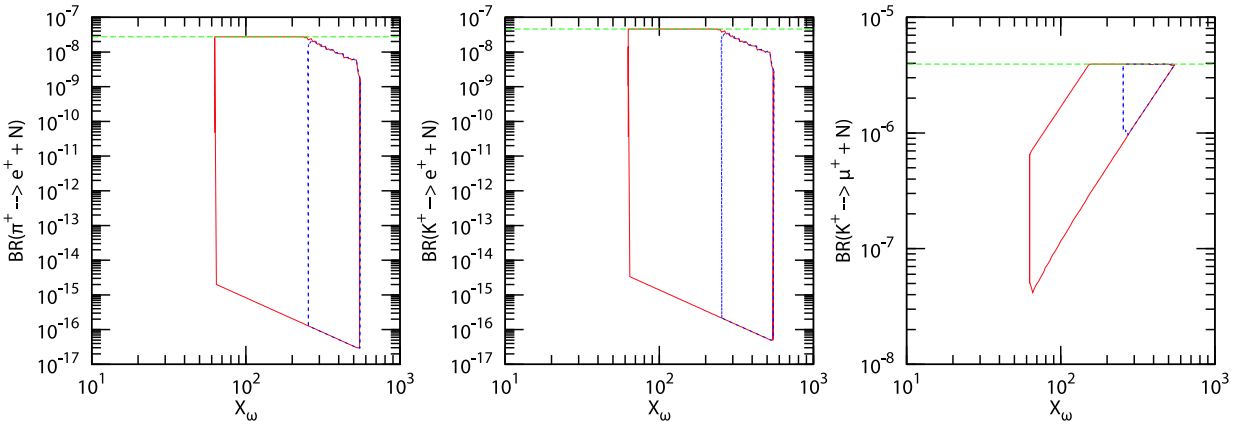

Figure 10: Allowed regions for the branching ratios of $\pi^+ \to e^+ + N_{2,3}$ (left), $K^+ \to e^+ + N_{2,3}$ (center), and $K^+ \to \mu^+ + N_{2,3}$ (right) in terms of X_ω for the NH case. The regions within the red solid lines and the blue dotted lines are allowed for the case when $\tau_{N_{2,3}} < 1$ sec and $\tau_{N_{2,3}} < \tau_{\rm BBN}$, respectively. The green horizontal lines represent the branching ratios when $|\Theta_{eI}| = |\Theta_{eI}|_{\rm UB}$ (left and center) and $|\Theta_{\mu I}| = |\Theta_{\mu I}|_{\rm UB}$ (right).

conditions (18) and (19) are satisfied, and hence the lower bounds on these branching ratios are also proportional to X_ω^{-2}. For large values of X_ω the upper bounds on these branching ratios are smaller than those evaluated by using the experimental upper bound $|\Theta_{eI}|^2_{\rm UB}$. This is because $|\Theta_{\mu I}|^2$ must take its maximal value $|\Theta_{\mu I}|^2_{\rm UB}$ to realize such a large X_ω, and then $|\Theta_{eI}\Theta_{\mu I}|_{\rm UB}$ in addition to $|\Theta_{\mu I}|^2_{\rm UB}$ forbids the case $|\Theta_{eI}|^2 = |\Theta_{eI}|^2_{\rm UB}$. On the other hand, the branching ratio of $K^+ \to \mu^+ + N_{2,3}$ cannot be so small since there is no cancellation in $|\Theta_{\mu I}|$ and also the larger value of $|\Theta_{\mu I}|$ is required for the shorter lifetime. Notice that $|\Theta_{\mu I}|^2$ cannot be large as $|\Theta_{\mu I}|^2_{\rm UB}$ for smaller values of X_ω. This is the reason why the upper bound on ${\rm BR}(K^+ \to \mu^+ + N_{2,3})$ is smaller than that evaluated by $|\Theta_{\mu I}|^2 = |\Theta_{\mu I}|^2_{\rm UB}$ when $X_\omega \lesssim 150$.

Therefore, we arrive at significant conclusions on the direct searches of $N_{2,3}$ in the NH case. By the peak search of positrons in π^+ or K^+ decays we would miss N_2 and N_3, since the model predicts too small branching ratios of these decays in some cases. Further, even if this is the case, it is possible to detect $N_{2,3}$ in the μ^+ spectrum in the K^+ decays. Interestingly, the future experiments of ${\rm BR}(K^+ \to \mu^+ + N_{2,3})$ improved the sensitivity by two orders of magnitude can cover the whole parameter space when $\tau_{N_{2,3}} < 1$ sec.

In the IH case, as shown in Fig. 11, the regions of the branching ratios are different from those in the NH case. Especially, the branching ratios, $\pi^+ \to e^+ + N_{2,3}$ and $K^+ \to e^+ + N_{2,3}$ cannot be so small as in the NH case due to the absence of the cancellation in $|\Theta_{eI}|$. Further, it should be noted that the model predict the branching ratio of $K^+ \to \mu^+ + N_{2,3}$ below the value with $|\Theta_{\mu I}|^2 = |\Theta_{\mu I}|^2_{\rm UB}$ for all the range of X_ω. The reason for small values of X_ω is the same as the NH case. In addition, the ratio $|\Theta_{eI}|/|\Theta_{\mu I}|$ cannot be very small in the IH case, and then the stringent experimental bound $|\Theta_{eI}|^2_{\rm UB}$ forbids $|\Theta_{\mu I}|^2$ being large as $|\Theta_{\mu I}|^2_{\rm UB}$. This leads to the experimental signature of the IH case, *i.e.*, the suppressed branching ratio of $K^+ \to \mu^+ + N_{2,3}$. In the IH case, therefore, the improvements of the experiments by one order

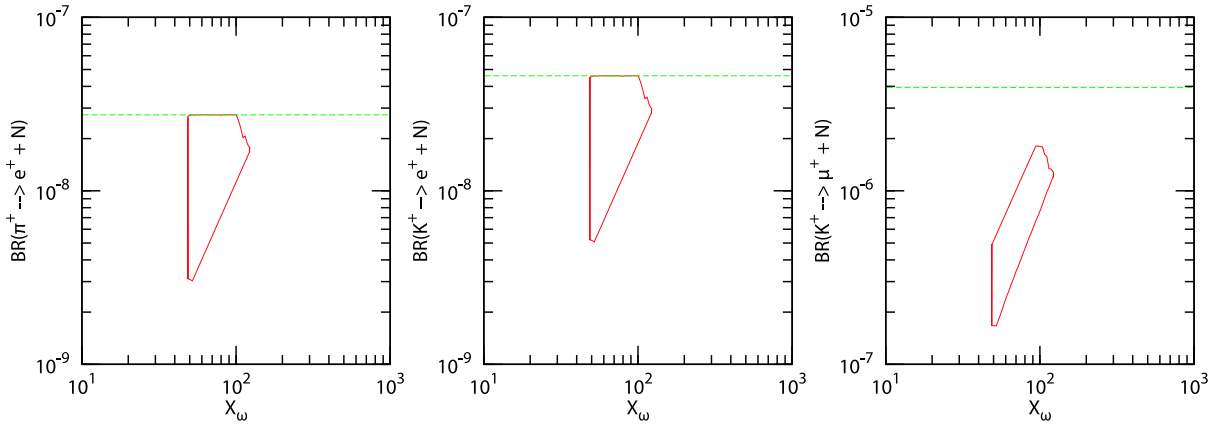

Figure 11: Allowed regions for the branching ratios of $\pi^+ \to e^+ + N_{2,3}$ (left), $K^+ \to e^+ + N_{2,3}$ (center), and $K^+ \to \mu^+ + N_{2,3}$ (right) in terms of X_ω for the IH case. The regions with the red solid lines are allowed for the case when $\tau_{N_{2,3}} < 1$ sec. The green horizontal lines represent the branching ratios when $|\Theta_{eI}| = |\Theta_{eI}|_{\rm UB}$ (left and center) and $|\Theta_{\mu I}| = |\Theta_{\mu I}|_{\rm UB}$ (right).

of magnitude can cover the whole parameter range when $\tau_{N_{2,3}} < 1$ sec for all the three decay channels.

Finally, we show in Figs. 12 and 13 the allowed ranges of the branching rations in terms of M_N for the NH and IH cases, respectively. Here we also impose the lifetime bound and vary the parameters of the model including X_ω. In the NH case, we find that the lower bounds on the branching ratios $\pi^+ \to e^+ + N_{2,3}$ and $K^+ \to e^+ + N_{2,3}$ are the same between two cases when $\tau_{N_{2,3}} < 1$ sec and $\tau_{N_{2,3}} < \tau_{\rm BBN}$. This is because such bounds are obtained by the largest X_ω as shown in Fig. 10. It is also find that the upper bound for $\tau_{N_{2,3}} < \tau_{\rm BBN}$ is slightly smaller than that for $\tau_{N_{2,3}} < 1$ sec. On the other hand, the upper bound on the branching ratio of $K^+ \to \mu^+ + N_{2,3}$ does not change by the lifetime bound. In contrast, the lower bound becomes much severer by the stringent lifetime bound $\tau_{N_{2,3}} < \tau_{\rm BBN}$. Therefore, the improvement in the measurement of ${\rm BR}(K^+ \to \mu^+ + N_{2,3})$ by a factor of 5 (by $\mathcal{O}(10^2)$) is sufficient to cover the allowed region with $\tau_{N_{2,3}} < \tau_{\rm BBN}$ ($\tau_{N_{2,3}} < 1$ sec) for 60 MeV $\lesssim M_N \lesssim$ 130 MeV. In the IH case, for all three decay channels, the improvement in the measurements by one or two orders of magnitude allows to cover the allowed region for 60 MeV $\lesssim M_N \lesssim$ 130 MeV.

Before closing this section, we would like to remark the following two points. First, the properties of the mixing elements $\Theta_{\alpha I}$ obtained in Sec. 3 are independent of the choice of the masses $M_{2,3}$. Therefore, the above arguments can be applied to sterile neutrinos heavier than pion mass. It should be stressed in particular that we have to pay a special attention to the processes of $N_{2,3}$ associated with electron/positron because of the cancellation in Θ_{eI} for the NH case. Second, we would like to comment again that, although we consider the νMSM in this paper, most of the results still hold for the general models of the seesaw mechanism with two right-handed neutrinos.

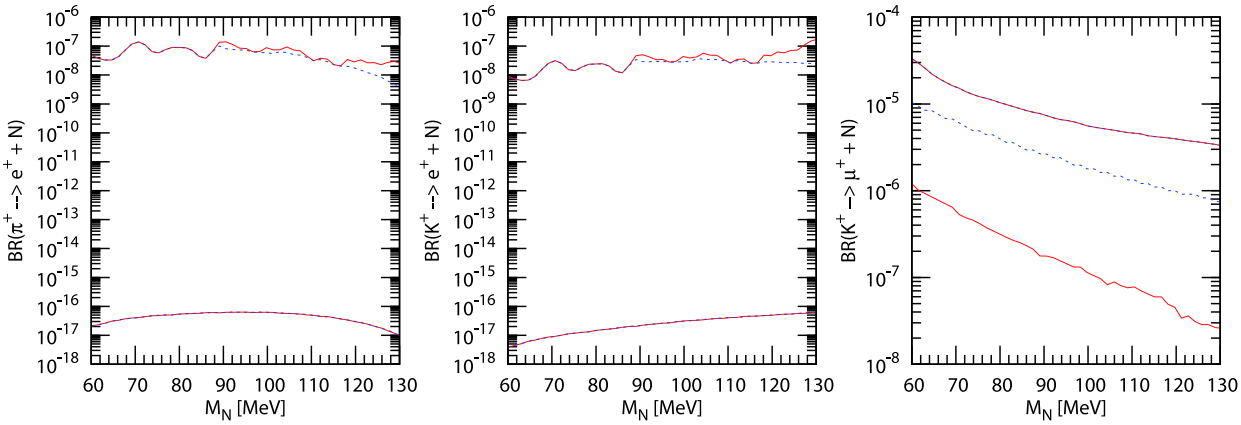

Figure 12: Allowed regions of the branching ratios of $\pi^+ \to e^+ + N_{2,3}$ (left), $K^+ \to e^+ + N_{2,3}$ (center), and $K^+ \to \mu^+ + N_{2,3}$ (right) in terms of M_N for the NH case. The regions within the red solid lines and the blue dotted lines are allowed for the case when $\tau_N < 1$ sec and $\tau_N < \tau_{\rm BBN}$ (46).

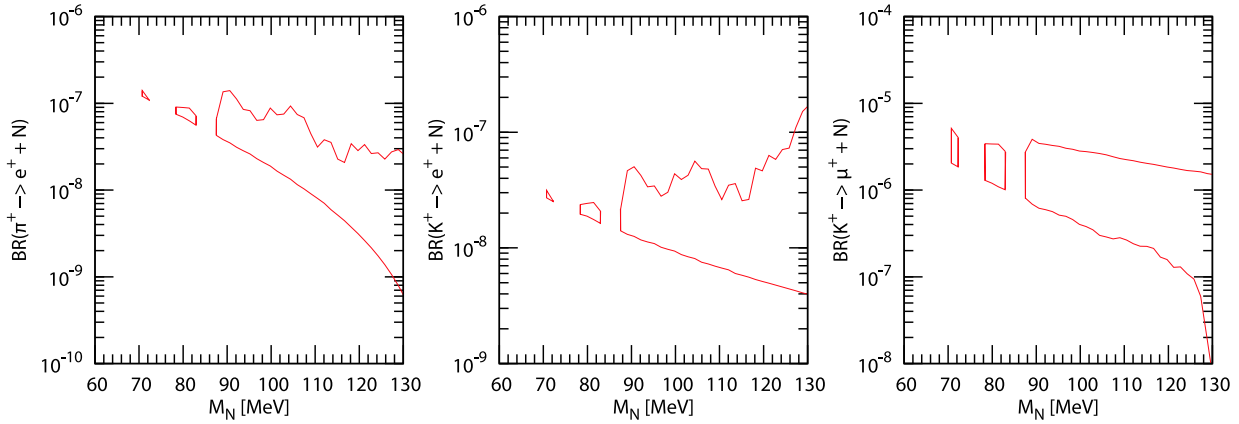

Figure 13: Allowed regions of the branching ratios of $\pi^+ \to e^+ + N_{2,3}$ (left), $K^+ \to e^+ + N_{2,3}$ (center), and $K^+ \to \mu^+ + N_{2,3}$ (right) in terms of M_N for the IH case. The regions within the red solid lines are allowed with $\tau_N < 1$ sec.

6 Conclusions

We have discussed mixing of active and sterile neutrinos in the νMSM, paying special attention to the mixing elements, $\Theta_{\alpha 2}$ and $\Theta_{\alpha 3}$, of N_2 and N_3. In this model, these sterile neutrinos are responsible to generate the seesaw mass matrix of active neutrinos as well as the baryon asymmetry of the universe through the mechanism of neutrino oscillation. Since these mixing elements are crucial to determine the strength of interaction of $N_{2,3}$, we have investigated the properties of $\Theta_{\alpha 2}$ and $\Theta_{\alpha 3}$ in detail.

It has been shown that the parameter Imω (or X_ω) is important to determine the overall scale of the Yukawa couplings of neutrinos. The couplings of $N_{2,3}$ scales as $|F_{\alpha I}| \propto e^{|{\rm Im}\omega|}$ and changes by orders of magnitude for $|{\rm Im}\omega| \gg 1$. We should stress again that the choice of Imω

does not change the masses and mixing angles of active neutrinos. Thus, the mixing elements $|\Theta_{\alpha I}|$ of $N_{2,3}$ can be larger as $|\mathrm{Im}\omega|$ becomes large, being consistent with the oscillation data.

We have then presented how the mixing elements depend on the neutrino parameters, namely masses, mixing angles and CP phases of active neutrinos. Interestingly, we have observed in the NH case that the leading terms of $|\Theta_{e2}|$ and $|\Theta_{e3}|$ vanish at the same time and they becomes suppressed as X_ω^{-2} for the large X_ω region, if the conditions (18) and (19) are satisfied. This is our important result, which is illustrated in Fig. 1. In order to realize this cancellation or the strong suppression in $|\Theta_{e2}|$ and $|\Theta_{e3}|$, the large value of θ_{13} is required. Thus, the experiments, *e.g.*, Double Chooz, T2K, RENO, Daya Bay, and NOνA in near future [65] will check whether it can happen in nature or not. The similar cancellation or suppression in $|\Theta_{e2}|$ and $|\Theta_{e3}|$ are potentially possible in the IH case. However, we have shown that the required conditions cannot be satisfied within the current neutrino data with 3σ error.

We have also discussed the $0\nu2\beta$ decays in the νMSM. Both contributions from active neutrinos and sterile neutrinos are fully taken into account. It has been found that quasi-degenerate sterile neutrinos N_2 and N_3 generating the baryon asymmetry of the universe gives a significant effect when their masses are smaller than about 100 MeV which is the typical energy scale in the nuclear matrix elements of the decays. In fact, when their masses are well below 100 MeV, the effective neutrino mass in the $0\nu2\beta$ decays vanishes in the νMSM, as already pointed out in Ref. [50] by using the general seesaw model. Moreover, when their masses are comparable to 100MeV, sterile neutrinos, N_2 and N_3, give destructive contribution and then $m_{\rm eff}$ becomes much smaller than that from active neutrinos. In this case, therefore, the $0\nu2\beta$ decays are suppressed due to the existence of light sterile neutrinos. Inversely speaking, the constraints from the $0\nu2\beta$ decays on the parameters of the νMSM become weaker in this mass region. On the other hand, when N_2 and N_3 are much heavier than 100 MeV, the contributions to the $0\nu2\beta$ decays from sterile neutrinos are negligible and $m_{\rm eff}$ is mainly comes from three active neutrinos as in the conventional seesaw model.

Moreover, we have estimated the lifetimes of N_2 and N_3 with $M_{2,3} < m_\pi$. It has been found that the lifetime can be shorter by taking large X_ω due to the enhancements of the mixing elements. As shown in Fig. 8, the present experimental limits on the mixing elements pose the lower bound on the lifetime as 10^{-2} sec at $M_N \simeq 120$ MeV in the NH case and 10^{-1} sec at $M_N \simeq 120$ MeV in the IH case. The obtained result is essential for the discussion of the cosmological constraints on the decays of N_2 and N_3. Especially, we have pointed out that, even if one imposes the current cosmological bound from the BBN as $\tau_{N_{2,3}} < \tau_{\rm BBN}$, there exists an allowed region for such light sterile neutrinos in the NH case. This is because of the cancellation in $|\Theta_{eI}|$ obtained in the present analysis. We have then derived the predictions on neutrino parameters, namely, θ_{13} is large, $\xi \sin(\delta + \eta) \simeq -1$, and $\xi \sin\eta < 0$. When we take the weaker bound as $\tau_{N_{2,3}} < 1$ sec, there are the allowed regions for both NH and IH cases.

Finally, we have investigated the direct search of N_2 and N_3 with $M_{2,3} < m_\pi$ in meson decays. Our study shows that, in the NH case, the experiments by using $\pi^+ \to e^+ + N_{2,3}$

and $K^+ \to e^+ + N_{2,3}$ would miss $N_{2,3}$ when θ_{13} is large. This is because the cancellation or strong suppression in Θ_{eI} can happen. In such a case, the peak search of the kaon decays $K^+ \to \mu^+ + N_{2,3}$ is crucially important to find $N_{2,3}$ having sizable mixing elements $\Theta_{\mu I}$. We should also comment that $N_{2,3}$ with $M_N \lesssim 55$ MeV is hard to find in the NH case, if the cancellation in Θ_{eI} happens. This is because the peak search in $K^+ \to \mu^+ + N_{2,3}$ is difficult for such a small mass region. On the other hand, in the IH case, all the three decay channels, $\pi^+ \to e^+ + N_{2,3}$, $K^+ \to e^+ + N_{2,3}$, and $K^+ \to \mu^+ + N_{2,3}$, are promising for the future experiments finding N_2 and N_3.

Acknowledgments

We would like to thank M. Shaposhnikov for useful discussions. The work of T.A. was partially supported by the Ministry of Education, Science, Sports and Culture, Grant-in-Aid for Scientific Research, No. 21540260, and by Niigata University Grant for Proportion of Project.

A Mixing elements $|\Theta_{\alpha I}|^2$ at $\mathcal{O}(X_\omega^2)$

In this appendix, we shall present the expressions of the mixing elements $|\Theta_{\alpha I}|^2$ at the $\mathcal{O}(X_\omega^2)$. In the NH case, we parameterize $|\Theta_{\alpha I}|^2$ at the $\mathcal{O}(X_\omega^2)$ as

$$|\Theta_{\alpha I}|^2\big|_{X_\omega^2} = \frac{X_\omega^2\, m_3}{4M_I}\, A_\alpha\,, \tag{50}$$

where A_α $(\alpha = e, \mu, \tau)$ are found as $[r_{23} = (m_2/m_3)^{1/2}]$

$$A_e = \cos^2\theta_{13}\Big[\tan^2\theta_{13} + 2r_{23}\xi\sin(\delta+\eta)\sin\theta_{12}\tan\theta_{13} + r_{23}^2\,\sin^2\theta_{12}\Big]\,, \tag{51}$$

$$\begin{aligned} A_\mu = {} & \cos^2\theta_{13}\sin^2\theta_{23} + r_{23}\,\xi\Big[\cos\theta_{12}\cos\theta_{13}\sin 2\theta_{23}\sin\eta - \sin\theta_{12}\sin 2\theta_{13}\sin^2\theta_{23}\sin(\delta+\eta)\Big] \\ & + r_{23}^2\Big[\cos^2\theta_{12}\cos^2\theta_{23} + \sin^2\theta_{12}\sin^2\theta_{13}\sin^2\theta_{23} - \frac{1}{2}\sin 2\theta_{12}\sin 2\theta_{23}\sin\theta_{13}\cos\delta\Big]\,, \end{aligned} \tag{52}$$

$$\begin{aligned} A_\tau = {} & \cos^2\theta_{13}\cos^2\theta_{23} - r_{23}\,\xi\Big[\cos\theta_{12}\cos\theta_{13}\sin 2\theta_{23}\sin\eta + \sin\theta_{12}\sin 2\theta_{13}\cos^2\theta_{23}\sin(\delta+\eta)\Big] \\ & + r_{23}^2\Big[\cos^2\theta_{12}\sin^2\theta_{23} + \sin^2\theta_{12}\sin^2\theta_{13}\cos^2\theta_{23} + \frac{1}{2}\sin 2\theta_{12}\sin 2\theta_{23}\sin\theta_{13}\cos\delta\Big]\,. \end{aligned} \tag{53}$$

On the other hand, in the IH case, we

$$|\Theta_{\alpha I}|^2\big|_{X_\omega^2} = \frac{X_\omega^2\, m_2}{4M_I}\, B_\alpha\,, \tag{54}$$

where B_α $(\alpha = e, \mu, \tau)$ are found as $[r_{12} = (m_1/m_2)^{1/2}]$

$$B_e = \cos^2\theta_{12}\cos^2\theta_{13}\Big[\tan^2\theta_{12} - 2r_{12}\xi\sin\eta\tan\theta_{12} + r_{12}^2\Big]\,, \tag{55}$$

$$
\begin{aligned}
B_\mu = & \cos\theta_{12}^2\cos^2\theta_{23} + \sin^2\theta_{12}\sin\theta_{13}^2\sin^2\theta_{23} - \frac{1}{2}\sin 2\theta_{12}\sin 2\theta_{23}\sin\theta_{13}\cos\delta \\
& + r_{12}\xi\Big[(\cos 2\theta_{12}\cos\delta\sin\eta - \sin\delta\cos\eta)\sin 2\theta_{23}\sin\theta_{13} \\
& \qquad + \sin 2\theta_{12}(\cos^2\theta_{13}\sin^2\theta_{23} + \cos 2\theta_{23})\sin\eta\Big] \\
& + r_{12}^2\Big[\cos^2\theta_{23}\sin^2\theta_{12} + \cos^2\theta_{12}\sin^2\theta_{13}\sin^2\theta_{23} + \frac{1}{2}\sin 2\theta_{12}\sin 2\theta_{23}\sin\theta_{13}\Big]\,, \qquad (56)
\end{aligned}
$$

$$
\begin{aligned}
B_\tau = & \cos\theta_{12}^2\sin^2\theta_{23} + \sin^2\theta_{12}\sin\theta_{13}^2\cos^2\theta_{23} + \frac{1}{2}\sin 2\theta_{12}\sin 2\theta_{23}\sin\theta_{13}\cos\delta \\
& + r_{12}\xi\Big[(-\cos 2\theta_{12}\cos\delta\sin\eta + \sin\delta\cos\eta)\sin 2\theta_{23}\sin\theta_{13} \\
& \qquad + \sin 2\theta_{12}(\cos^2\theta_{13}\cos^2\theta_{23} - \cos 2\theta_{23})\sin\eta\Big] \\
& + r_{12}^2\Big[\sin^2\theta_{23}\sin^2\theta_{12} + \cos^2\theta_{12}\sin^2\theta_{13}\cos^2\theta_{23} - \frac{1}{2}\sin 2\theta_{12}\sin 2\theta_{23}\sin\theta_{13}\Big]\,. \qquad (57)
\end{aligned}
$$

References

[1] P. Minkowski, Phys. Lett. B **67** (1977) 421; T. Yanagida, in *Proc. of the Workshop on the Unified Theory and the Baryon Number in the Universe*, Tsukuba, Japan, Feb. 13-14, 1979, p. 95, eds. O. Sawada and S. Sugamoto, (KEK Report KEK-79-18, 1979, Tsukuba); Progr. Theor. Phys. **64** (1980) 1103 ; M. Gell-Mann, P. Ramond and R. Slansky, in *Supergravity*, eds. P. van Niewenhuizen and D. Z. Freedman (North Holland, Amsterdam 1980); P. Ramond, in *Talk given at the Sanibel Symposium*, Palm Coast, Fla., Feb. 25-Mar. 2, 1979, preprint CALT-68-709 (retroprinted as hep-ph/9809459); S. L. Glashow, in *Proc. of the Cargése Summer Institute on Quarks and Leptons*, Cargése, July 9-29, 1979, eds. M. Lévy et. al, , (Plenum, 1980, New York), p707.

[2] M. Fukugita and T. Yanagida, Phys. Lett. B **174** (1986) 45 .

[3] See, for reviews, *e.g.*, W. Buchmuller, R. D. Peccei and T. Yanagida, Ann. Rev. Nucl. Part. Sci. **55** (2005) 311 [arXiv:hep-ph/0502169]; S. Davidson, E. Nardi and Y. Nir, Phys. Rept. **466**, 105 (2008) [arXiv:0802.2962 [hep-ph]].

[4] For example, see G. F. Giudice, A. Notari, M. Raidal, A. Riotto and A. Strumia, Nucl. Phys. B **685** (2004) 89 [arXiv:hep-ph/0310123].

[5] T. Asaka, S. Blanchet and M. Shaposhnikov, Phys. Lett. B **631** (2005) 151.

[6] T. Asaka and M. Shaposhnikov, Phys. Lett. B **620** (2005) 17.

[7] A. de Gouvea, Phys. Rev. D **72** (2005) 033005 [arXiv:hep-ph/0501039].

[8] F. L. Bezrukov and M. Shaposhnikov, Phys. Lett. B **659** (2008) 703 [arXiv:0710.3755 [hep-th]].

[9] M. Shaposhnikov and I. Tkachev, Phys. Lett. B **639** (2006) 414 [arXiv:hep-ph/0604236].

[10] A. Kusenko, Phys. Rev. Lett. **97** (2006) 241301 [arXiv:hep-ph/0609081].

[11] A. Anisimov, Y. Bartocci and F. L. Bezrukov, Phys. Lett. B **671** (2009) 211 [arXiv:0809.1097 [hep-ph]].

[12] F. Bezrukov and D. Gorbunov, JHEP **1005** (2010) 010 [arXiv:0912.0390 [hep-ph]].

[13] F. Bezrukov, D. Gorbunov and M. Shaposhnikov, JCAP **0906** (2009) 029 [arXiv:0812.3622 [hep-ph]].

[14] P. J. E. Peebles, Astrophys. J. **258** (1982) 415; K. A. Olive and M. S. Turner, Phys. Rev. D **25** (1982) 213.

[15] A. Kusenko and G. Segre, Phys. Lett. B **396** (1997) 197 [arXiv:hep-ph/9701311]; G. M. Fuller, A. Kusenko, I. Mocioiu and S. Pascoli, Phys. Rev. D **68** (2003) 103002 [arXiv:astro-ph/0307267]; M. Barkovich, J. C. D'Olivo and R. Montemayor, Phys. Rev. D **70** (2004) 043005 [arXiv:hep-ph/0402259]; A. Kusenko, B. P. Mandal and A. Mukherjee, Phys. Rev. D **77** (2008) 123009 [arXiv:0801.4734 [astro-ph]].

[16] A. Kusenko, Phys. Rept. **481** (2009) 1 [arXiv:0906.2968 [hep-ph]].

[17] S. Dodelson and L. M. Widrow, Phys. Rev. Lett. **72** (1994) 17 [arXiv:hep-ph/9303287].

[18] X. D. Shi and G. M. Fuller, Phys. Rev. Lett. **82** (1999) 2832 [arXiv:astro-ph/9810076].

[19] A. D. Dolgov and S. H. Hansen, Astropart. Phys. **16** (2002) 339 [arXiv:hep-ph/0009083];

[20] K. Abazajian, G. M. Fuller and M. Patel, Phys. Rev. D **64** (2001) 023501 [arXiv:astro-ph/0101524];

[21] K. Abazajian, G. M. Fuller and W. H. Tucker, Astrophys. J. **562** (2001) 593 [arXiv:astro-ph/0106002];

[22] K. N. Abazajian and G. M. Fuller, Phys. Rev. D **66** (2002) 023526 [arXiv:astro-ph/0204293];

[23] K. Abazajian, Phys. Rev. D **73** (2006) 063506 [arXiv:astro-ph/0511630];

[24] C. T. Kishimoto, G. M. Fuller and C. J. Smith, Phys. Rev. Lett. **97**, 141301 (2006) [arXiv:astro-ph/0607403].

[25] T. Asaka, M. Laine and M. Shaposhnikov, JHEP **0701** (2007) 091 [arXiv:hep-ph/0612182].

[26] M. Shaposhnikov, JHEP **0808** (2008) 008 [arXiv:0804.4542 [hep-ph]].

[27] M. Laine and M. Shaposhnikov, JCAP **0806** (2008) 031 [arXiv:0804.4543 [hep-ph]].

[28] See, for example, a review and references therein A. Boyarsky, O. Ruchayskiy and M. Shaposhnikov, Ann. Rev. Nucl. Part. Sci. **59** (2009) 191 [arXiv:0901.0011 [hep-ph]].

[29] M. Viel, J. Lesgourgues, M. G. Haehnelt, S. Matarrese and A. Riotto, Phys. Rev. Lett. **97**, 071301 (2006) [arXiv:astro-ph/0605706].

[30] U. Seljak, A. Makarov, P. McDonald and H. Trac, Phys. Rev. Lett. **97**, 191303 (2006) [arXiv:astro-ph/0602430].

[31] A. Boyarsky, J. Lesgourgues, O. Ruchayskiy and M. Viel, JCAP **0905**, 012 (2009) [arXiv:0812.0010 [astro-ph]].

[32] A. Boyarsky, J. Lesgourgues, O. Ruchayskiy and M. Viel, Phys. Rev. Lett. **102**, 201304 (2009) [arXiv:0812.3256 [hep-ph]].

[33] F. L. Bezrukov and M. Shaposhnikov, Phys. Rev. D **75** (2007) 053005 [arXiv:hep-ph/0611352].

[34] E. K. Akhmedov, V. A. Rubakov and A. Y. Smirnov, Phys. Rev. Lett. **81** (1998) 1359.

[35] V. A. Kuzmin, V. A. Rubakov and M. E. Shaposhnikov, Phys. Lett. B **155** (1985) 36.

[36] T. Asaka and H. Ishida, Phys. Lett. B **692** (2010) 105 [arXiv:1004.5491 [hep-ph]].

[37] L. Canetti and M. Shaposhnikov, JCAP **1009** (2010) 001 [arXiv:1006.0133 [hep-ph]].

[38] D. Gorbunov and M. Shaposhnikov, JHEP **0710** (2007) 015 [arXiv:0705.1729 [hep-ph]].

[39] M. Shaposhnikov, Nucl. Phys. B **763** (2007) 49 [arXiv:hep-ph/0605047].

[40] F. L. Bezrukov, Phys. Rev. D **72** (2005) 071303 [arXiv:hep-ph/0505247].

[41] P. Benes, A. Faessler, F. Simkovic and S. Kovalenko, Phys. Rev. D **71**, 077901 (2005) [arXiv:hep-ph/0501295].

[42] A. D. Dolgov, S. H. Hansen, G. Raffelt and D. V. Semikoz, Nucl. Phys. B **580**, 331 (2000) [arXiv:hep-ph/0002223].

[43] A. D. Dolgov, S. H. Hansen, G. Raffelt and D. V. Semikoz, Nucl. Phys. B **590**, 562 (2000) [arXiv:hep-ph/0008138].

[44] B. Pontecorvo, Sov. Phys. JETP **7** (1958) 172;
Z. Maki, M. Nakagawa and S. Sakata, Prog. Theor. Phys. **28** (1962) 870.

[45] J. A. Casas and A. Ibarra, Nucl. Phys. B **618** (2001) 171 [arXiv:hep-ph/0103065].

[46] A. Abada, S. Davidson, A. Ibarra, F. X. Josse-Michaux, M. Losada and A. Riotto, JHEP **0609** (2006) 010 [arXiv:hep-ph/0605281].

[47] For example, see, T. Schwetz, M. A. Tortola and J. W. F. Valle, New J. Phys. **10** (2008) 113011 [arXiv:0808.2016 [hep-ph]].

[48] F. Feruglio, A. Strumia and F. Vissani, Nucl. Phys. B **637**, 345 (2002) [Addendum-ibid. B **659**, 359 (2003)] [arXiv:hep-ph/0201291];
M. Hirsch, arXiv:hep-ph/0609146.

[49] M. Hirsch and H. V. Klapdor-Kleingrothaus, *Prepared for International Workshop on Neutrinoless Double Beta Decay and Related Topics, Trento, Italy, 24 Apr - 5 May 1995*

[50] M. Blennow, E. Fernandez-Martinez, J. Lopez-Pavon and J. Menendez, JHEP **1007** (2010) 096 [arXiv:1005.3240 [hep-ph]].

[51] C. Aalseth *et al.*, arXiv:hep-ph/0412300.

[52] For example, see M. Kawasaki, K. Kohri and T. Moroi, Phys. Rev. D **71**, 083502 (2005) [arXiv:astro-ph/0408426].

[53] R. E. Shrock, Phys. Lett. B **96** (1980) 159.

[54] D. I. Britton *et al.*, Phys. Rev. D **46** (1992) 885.

[55] D. I. Britton *et al.*, Phys. Rev. Lett. **68** (1992) 3000.

[56] T. Yamazaki, in Proc. Neutrino '84 (Dortmund, 1984).

[57] R. S. Hayano *et al.*, Phys. Rev. Lett. **49** (1982) 1305.

[58] G. Bernardi *et al.*, Phys. Lett. B **166** (1986) 479.

[59] G. Bernardi *et al.*, Phys. Lett. B **203** (1988) 332.

[60] J. Orloff, A. N. Rozanov and C. Santoni, Phys. Lett. B **550** (2002) 8 [arXiv:hep-ph/0208075].

[61] A. Kusenko, S. Pascoli and D. Semikoz, JHEP **0511** (2005) 028 [arXiv:hep-ph/0405198].

[62] A. Atre, T. Han, S. Pascoli and B. Zhang, JHEP **0905** (2009) 030 [arXiv:0901.3589 [hep-ph]].

[63] T. Asaka, S. Eijima and H. Ishida, in preparation.

[64] L. M. Johnson, D. W. McKay and T. Bolton, Phys. Rev. D **56** (1997) 2970 [arXiv:hep-ph/9703333].

[65] See, for a review, M. Mezzetto and T. Schwetz, J. Phys. G **37**, 103001 (2010) [arXiv:1003.5800 [hep-ph]].